energies

MDPI

Article

Performance Analysis of a New Cogeneration System with Efficient Utilization of Waste Heat Resources and Energy Conversion Capabilities

Dahan Sun [1,*], Zhongyan Liu [2], Hao Zhang [2] and Xin Zhang [2]

[1] School of Energy Science and Engineering, Harbin Institute of Technology, Harbin 150001, China
[2] School of Energy and Power Engineering, Northeast Electric Power University, Jilin 132000, China; llzzyy198584@126.com (Z.L.); zhanghao9709@163.com (H.Z.); zhangxinxy4@163.com (X.Z.)
* Correspondence: hitdhsun@163.com

Abstract: This paper proposes a new type of cogeneration system coupled by Organic Rankine Cycle (ORC), Absorption Heat Pump (AHP), and Compression Heat Pump (CHP). The new system can meet the needs of different scenarios. Simulations were conducted to analyze the effect of different factors on the parameters and performance indexes of the new system and compared with the system of ORC, AHP, CHP. The results showed that the factors of flue gas temperature at evaporator1 outlet and CHP have the greatest effect on the parameters and performance indexes of the Organic Absorption-Compression Coupling Heat Power (OACCHP) system, and the effect of AHP on the parameters and performance indexes of the OACCHP system can be ignored. In the given range of flue gas temperature at evaporator1 outlet, the heat production of total and net work is reduced by 1.17% and 33.33%, respectively. In a given range of CHP evaporation temperature, the heat production of the total is reduced by 5.74%. In the given range of the outlet temperature of the gas cooler, the heat production of the total is increased by 10.58%. In a given working condition, compared with the single ORC system, the single CHP system, and the single AHP system, the thermal efficiency, COP, and energy earning rate of the OACCHP system are increased by up to 755.49%, 59.8%, 5.8%, respectively. Finally, the optimal operating conditions for different scenarios were determined.

Keywords: new cogeneration system; coefficient of performance; thermal efficiency; energy earning rate; waste heat utilization

check for updates

Citation: Sun, D.; Liu, Z.; Zhang, H.; Zhang, X. Performance Analysis of a New Cogeneration System with Efficient Utilization of Waste Heat Resources and Energy Conversion Capabilities. *Energies* **2024**, *17*, 3347. https://doi.org/10.3390/en17133347

Academic Editor: María Pilar Lisbona

Received: 21 August 2023
Revised: 1 September 2023
Accepted: 6 October 2023
Published: 8 July 2024

Copyright: © 2024 by the authors. Licensee MDPI, Basel, Switzerland. This article is an open access article distributed under the terms and conditions of the Creative Commons Attribution (CC BY) license (https://creativecommons.org/licenses/by/4.0/).

1. Introduction

At present, energy shortages and environmental degradation have become global concerns, and accelerating the development of clean energy is the key to solving these problems. In recent years, the development and utilization of waste heat resources have attracted widespread attention [1,2]. Compared to traditional clean energy, waste heat resources are considered good clean energy and zero carbon heat sources due to the lack of additional direct carbon emissions [3]. At the same time, there are various types and significant quantities of waste heat resources, such as waste heat from internal combustion engines [4], biomass flue gas [5], waste heat from gas turbines [6], and industrial waste gas [7].

In terms of waste heat recovery and utilization, direct heat exchange between waste heat and water is a traditional method of waste heat recovery. However, the waste heat utilization rate of this method is low, depends on the temperature of the waste heat source, and fails to achieve energy improvement and conversion. Therefore, many scholars have shifted their research focus to more efficient and widely applied ORC (organic Rankine cycle), heat pumps, and cogeneration technologies.

In terms of ORC technology, Song et al. [8] conducted research on using ORC technology to recover waste heat from a marine diesel engine. The maximum net power output was selected as the evaluation standard, and the best system parameters were determined. The results showed that the optimized system had certain advantages in both technology and economy. Mikielewicz et al. [9] conducted research on the ORC device for recovering waste heat from the waste gas of power generation units and used four different working fluids. The results showed that when ethanol was used as the working fluid, the thermal efficiency of ORC was the highest. Loni et al. [10] summarized and discussed the research of organic Rankine cycle (ORC) in industrial waste heat recovery. The results showed that using waste heat was an attractive and efficient way to generate electricity, and cogeneration with waste heat was also a good alternative design because it could improve the overall efficiency and optimize the utilization of waste heat. Sun et al. [11] proposed an ORC coupling device that can recover waste heat from the CO_2 refrigeration system and analyzed the impact of different factors on system performance. The results showed that the addition of ORC device could effectively improve the system performance, and the outlet temperature of the first-stage gas cooler had the greatest impact on COP. Nondy et al. [12] studied four different organic Rankine cycle structures from the perspective of sports economy. The results showed that compared to the basic ORC, the net power and exergy efficiency of the RR-ORC were higher, while the system cost rate was lower. Soltani et al. [13] conducted a comparative study on the organic Rankine cycle and Kalina cycle from the perspectives of the first and second laws of thermodynamics. The results showed that when R290 was used as the working fluid for ORC, the system had the highest waste heat recovery and increased production capacity by 2.47%. Wang et al. [14] proposed a system that utilizes ORC to recover waste heat for hydrogen production and established a comprehensive thermodynamic model. The results showed that the system could produce hydrogen at a rate of 0.431 kg/s and a power output of 32,386.45 kW with a power reduction of 60%. Wei et al. [15] optimized the system performance of the organic Rankine cycle (ORC) system and analyzed the thermodynamic performance of the ORC system under disturbances. The results showed that when the ambient temperature was too high, the net power and efficiency output of the system would decrease, and the deviation from the nominal state may exceed 30%. Wang et al. [16] conducted research on the use of ORC to recover exhaust heat from automotive engines and determined the optimal working fluid selection. The results showed that the thermodynamic performance of R11, R141b, R113, and R123 were higher, and R245fa and R245ca were the most environment-friendly working fluids. Alghamdi et al. [17] established a joint dual flash geothermal cycle power generation model and conducted a comprehensive thermodynamic analysis, and the working fluid of ORC adopts azeotropic working fluid. Then, the pure fluid model results were compared with previous research results. Finally, a series of important parameters, such as cycle efficiency, were obtained and compared.

In terms of heat pump technology, it is mainly divided into compression heat pumps and absorption heat pumps. Cao et al. [18] used different heat pump systems to recover heat from wastewater with an average temperature of 45 °C and conducted thermodynamic and economic analyses on each system. The results showed that the COP (coefficient of performance) and exergy efficiency for two-stage heat pump with flash tank and two-stage heat pump with flash tank and intercooler were much higher than those of other systems. Hu et al. [19] proposed a new type of centrifugal heat pump system to recover waste heat from steel plants. The system used two steam jet centrifugal compressors and a two-cycle parallel system configuration. The results showed that when the temperature rise exceeded 30 °C, the COP was expected to exceed 6, and the PER of the megawatt compression heat pump was as high as 2.53, and the payback period of this waste heat recovery system was 1.66 years. Mateu-Royo et al. [20] studied eight advanced cycle configurations for recovering industrial waste heat from the perspectives of energy, economy, and environment. They determined the optimal choice for different high-temperature and high-pressure applications. The results showed that when the temperature rise was 60 K or above, a two-stage

cascade was the best choice, when the temperature rise was 50 K or less, a single-stage cycle was the best choice. Hou et al. [21] proposed a boiler flue gas waste heat recovery system driven by different heat sources, and the driving heat sources were hot water and flue gas generated by the boiler. The results showed that the system could reduce the flue gas temperature from 120 °C to below 30 °C, and the boiler efficiency could be improved by 11.8%. Lars et al. [22] used open absorption heat pump technology to study biomass boiler flue gas purification and energy recovery systems, and the flue gas flowed through a generator, a direct contact flue gas heat exchanger, and an absorber in sequence. The results showed that the system could reduce large particulate matter in flue gas by 33–44%, and small particulate matter could also be removed to a certain extent. At the same time, when wet fuel was used, the heat production increased by 40%. Xu et al. [23] proposed the use of dual-stage lithium bromide absorption heat pumps for low-grade waste heat recovery, and the temperature of the heat source and the temperature of the waste water were 120.1 °C and 45 °C, respectively. The results showed that the temperature of the waste water could be reduced by 29.1 °C, and 52.5 °C hot water can be output for household heating. At the same time, the capacity and COP of the system were 8666.4 kW and 1.77, respectively. Ma et al. [24] proposed a new type of a absorption-compression hybrid heat pump system and compared it to traditional heat pump systems. The results showed that the system could recover waste heat within the temperature range of 60–120 °C and upgraded ultra-low grade waste heat within the temperature range of 40–60 °C by using an absorption heat exchange transformer. Yang et al. [25] proposed a system that couples the lithium bromide absorption refrigeration cycle and transcritical CO_2 cycle and simulated the effects of condensation temperature, high pressure, and other parameters on system performance. The results showed that the system can recover low-grade waste heat at 90–150 °C. Sun et al. [26] proposed a two-stage evaporation absorption heat pump and conducted simulation and experimental research under low waste heat temperature conditions. The results showed that compared to ordinary plate heat exchangers, the recovery period of this system can be shortened by two years. Assad et al. [27] conducted a comprehensive study on the performance of a single effect H_2O/LiBr absorption chiller driven by geothermal energy. The results showed that when the production well temperature is 250 °C, separator pressure is 0.24 MPa, and condenser pressure is 7.5 KPa, the thermal efficiency of the system is about 13%. When the geofluid temperature is 120 °C, and the efficiency of the solution heat exchanger is 0.9, the COP is about 0.87.

In terms of cogeneration technology, Chang et al. [28] proposed a cogeneration system that can be used to recover waste heat from PEMFC. The results showed that the average COP of the cogeneration system was 1.19 in summer and 1.42 in winter, and the current density and operating temperature have significant effects on the performance of the cogeneration system. Pan et al. [29] proposed a new type of cogeneration system that can effectively recover waste heat from garbage and conducted a comprehensive thermodynamic analysis of the system. The results showed that the evaporator temperature of HP, the superheat of HP evaporator, and ambient temperature had a greater impact on system, and the specific investment cost was reduced from 333.15 to 325.94 $/GJ. Amir Ebrahimi-Moghadam et al. [30] conducted a sensitivity analysis and multi-objective optimization on a novel combined cogeneration system. The results showed that the total exergy destruction was reduced by 3.65% after optimization. Xie et al. [31] designed a 1 kW PEMFC-based residential micro-cogeneration system and studied the energy and exergy performance of the system. The results showed that for the typical case, energy carried by unuseful streams accounts for the majority of the energy and exergy losses, and proton exchange membrane fuel cells posses the least energy efficiency and exergy efficiency. Obi et al. [32] conducted a comprehensive literature review on micro cogeneration systems below 100 kW by considering the effects of environment and working fluid properties and discussed the selection criteria for working fluids. The results showed that the most commonly used fluid in ORC systems was R245fa, and a detailed list of characteristics of both industrial and experimental prototype applications was presented. Holik et al. [33] proposed a cogeneration

system that can recover waste heat from engine exhaust and conducted multi-objective optimization analysis on the system. The results showed that the electrical efficiency of the system was 42.1%, the annual total energy efficiency was 66.7%, and the optimized power efficiency had increased by 2.97%. Pantaleo et al. [34] conducted a comparative study on the system performance of a (cogeneration + MGT prime mover) and a (waste heat recovery + ORC engine). The results showed that natural gas, electricity prices, and coffee roasting production capacity were key factors affecting profitability, and the cogeneration solution via an MGT appeared as a more profitable option than waste-heat recovery via an ORC engine primarily. Su et al. [35] developed a new and efficient cogeneration system that can recover waste heat and capture carbon and analyzed the performance, synergy, sensitivity, and dehumidification ability of the system. The results showed that when the system was applied to coal-fired power plant, the power generation, thermal efficiency, dehumidification rate, and carbon capture capacity of coal-fired power plant had increased by 13.34% and 5.74%, 15.69 g/kg and 130.99 kg/s, respectively. Liu et al. [36] proposed a competitive cogeneration system that combined organic Rankine cycles with heat pump cycles through a "built-in" evaporator and compared it with traditional systems. The results showed that the thermal efficiency and waste heat recovery efficiency of the new system were increased by 6.4% and 1.2%, respectively. In addition, the thermal efficiency of the system increased linearly, and the waste heat recovery efficiency changed as a quadratic function with the increase in evaporation temperature. Zhang et al. [37] proposed a new type of air-cooled gas-steam combined cycle cogeneration system with absorption heat pump for recovering waste heat from the exhausted steam of the steam turbine. The results showed that the net power generation was increased by approximately 11,082 kW, equivalent coal consumption was decreased by 2.71 g/kWh, and the net total thermal efficiency was increased by 0.91%. Li et al. [38] proposed a new type of cogeneration heating system and compared the new system with other systems in terms of thermodynamics, energy consumption and economy. The results showed that compared with other systems, the total energy efficiency of the new cogeneration heating system was improved by 6.1–14.1%, the equivalent electrical energy for heating was reduced by 11.1–29.4%, and the unit heating cost was reduced by 8.7–23.9%.

In summary, many scholars have conducted more research on the use of ORC, heat pump, and cogeneration technologies to recover waste heat, and these studies have also improved energy utilization from different perspectives. However, for ORC systems, the condensation waste heat is not well utilized, resulting in the waste of low-grade heat energy, and the system is limited by the temperature of the heat source. For heat pump systems, although they can achieve the upgrading of low-grade thermal energy, they fail to convert thermal energy into other types of energy, making their application scenarios relatively single. For the cogeneration systems, although they combine the advantages of ORC and heat pump systems, there are very few existing research on cogeneration systems that can achieve gradient utilization of waste heat, resulting in insufficient utilization of waste heat resources.

In response to the above issues, this paper proposes a new type of cogeneration system that can utilize waste heat resources from multiple perspectives. The new system is composed of an ORC system, a compression heat pump (CHP) system, and an absorption heat pump (AHP) system coupled together. The new system not only effectively utilizes the condensed waste heat in the ORC system but also achieves gradient utilization of waste heat, achieving full utilization of waste heat resources from multiple perspectives, providing a certain reference for the utilization of waste heat resources and the development of cogeneration systems in the future.

This paper first establishes a new system model and thermodynamic calculation model and then focuses on analyzing the impact of different factors on system parameters and performance indexes based on the first law of thermodynamics. At the same time, it is also compared with traditional ORC, compression heat pump, and absorption heat pump.

Finally, the optimal operating conditions of the system are determined based on different application scenarios and objectives.

2. System Introduction and Model Establishment

2.1. System Description

Figure 1 shows the diagram of the new heating and power system, namely the ORC-AHP-CHP coupled heating and power (OACCHP) system. The new system consists of an organic Rankine cycle (ORC), an absorption heat pump (AHP) cycle, and a compression heat pump (CHP) cycle, respectively. The heat source of the system consists of the main heat source and auxiliary heat source, with flue gas waste heat as the main heat source, and the condensation waste heat of ORC as the auxiliary heat source. The flue gas waste heat sequentially passes through the evaporator in ORC, the generator in AHP, the evaporator in AHP, and the flue gas heat exchanger in CHP, achieving a four-stage gradient recovery and utilization of flue gas waste heat. At the same time, the evaporator in CHP recovers the condensation waste heat in ORC, further achieving multi-directional utilization of heat energy. In the new system, the ORC uses R245fa as the cycling working fluid. The cycling working fluid of AHP is LiBr solution, and the refrigerant is water. The refrigerant of CHP is CO_2. The specific thermophysical parameters of each working fluid are shown in Table 1.

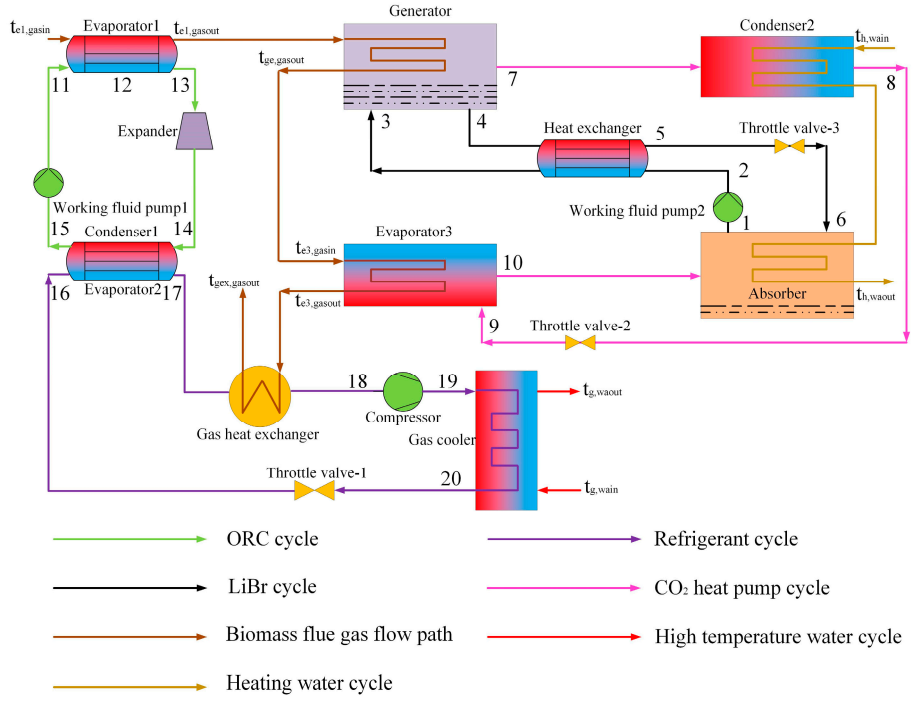

Figure 1. System diagram of the ORC-AHP-CHP coupled heating and power system.

Table 1. The thermophysical parameters of each working fluid.

Parameter	CO_2	R245fa	Water
Critical pressure	7.37 MPa	3.65 MPa	22.06 MPa
Critical temperature	304.13 K	427.16 K	647.1 K
Molar mass	44.01 kg/kmol	134.05 kg/kmol	18.01 kg/kmol
Normal Boiling Point	194.69 K	288.29 K	373.12 K

Figure 2 shows the *P-h* diagram of ORC and CHP cycle in the new system, and Figure 3 shows the *h-x* diagram of AHP cycle. In the new system, 1–2 is the pressurization process of the weak solution; 2–3 is the preheating process of the weak solution; 3–4 (7) indicate that the weak solution absorbs the heat source temperature for concentration and generates water vapor, 3–3g is the pressure change process of the weak solution entering the

generator, and 3g–4 is the process of the weak solution becoming a strong solution; 4–5 is the exothermic process of a strong solution; 5–6 is the throttling and depressurization process of strong solution; 6–1 (10) indicates that the strong solution absorbs water vapor for dilution and releases a large amount of heat, 6–6a is the pressure change process of the strong solution entering the absorber, and 6a–1 is the process of the strong solution becoming a weak solution; 7–8 is the condensation exothermic process; 8–9 is the isoenthalpy throttling process; 9–10 is the evaporation endothermic process; 11–13 is the evaporative endothermic process; 13–14 is the actual expansion process; 13–14s is the isentropic expansion process; 14–15 is the condensation exothermic process; 15–11 is the actual pressurization process; 15–11s is the isentropic pressurization process; 16–17 is the first stage of CO_2 evaporation endothermic process; 17–18 is the second stage of CO_2 evaporation endothermic process; 18–19s is the isentropic compression; 18–19 is the actual compression; 19–20 is the isobaric cooling process; 20–16 is the isoenthalpy throttling process.

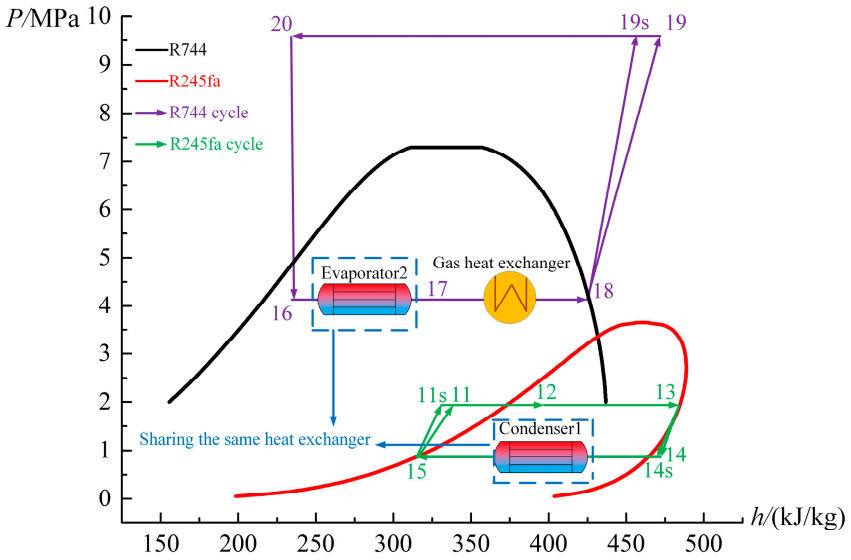

Figure 2. *P-h* diagram of ORC and CHP cycle.

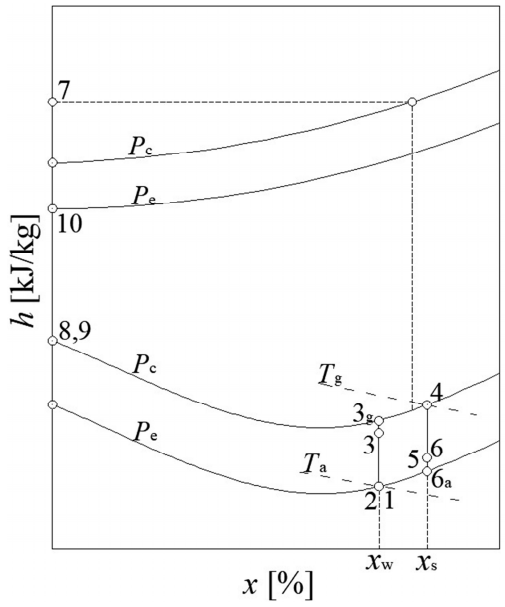

Figure 3. *h-x* diagram of AHP cycle.

2.2. Physical Properties of Working Fluid

Table 1 shows the thermophysical parameters of each working fluid in the new system, and the thermophysical properties of CO_2, R245fa, and water were all obtained from REFPROP9.0 [39], and the relevant thermophysical properties of LiBr aqueous solution were calculated by EES software (EES pro 10.56). Table 2 shows the ODP and GWP values of each working fluid.

Table 2. The ODP and GWP of each working fluid.

Parameters	CO_2	Water	R245fa
ODP	0	0	0
GWP	1	0	790

2.3. Model Assumptions

All the analyses in this paper are based on the following assumptions:

(1) The system is in steady state;
(2) When the working fluid flows in the heat exchanger and connecting pipe, the pressure drop and heat loss are not considered;
(3) The compression process is adiabatic but not isentropic;
(4) State points 7, 8, 10, 13, 15, 18 are saturated;
(5) The refrigerant does not contain lubricating oil;
(6) The pressure of condenser2 and generator is the same, the pressure of the absorber and evaporator3 is the same;
(7) The power consumption, concentration, temperature, enthalpy, and entropy before and after throttle valve3 and working fluid pump2 are not considered;

2.4. Energy Thermodynamic Model

The energy analysis is only based on the changes in refrigerant parameters and is not related to the parameters of the external environment.

Energy thermodynamic model

1. CHP cycle system:

(i) Work input to compressor:

$$W_{com} = m_{CO_2}(h_{19} - h_{18}) = m_{CO_2}(h_{19s} - h_{18})/\varepsilon_{is} \quad (1)$$

(ii) Heating effect of gas cooler:

$$Q_g = m_{CO_2}(h_{20} - h_{19}) \quad (2)$$

(iii) Refrigerating effect of evaporator2:

$$Q_{e2} = m_{CO_2}(h_{17} - h_{16}) \quad (3)$$

(iv) Refrigerating effect of gas heat exchanger:

$$Q_{gex} = m_{CO_2}(h_{18} - h_{17}) \quad (4)$$

(v) Mass flow of CO_2:

$$m_{CO_2} = \frac{m_{R245fa} \cdot (h_{14} - h_{15}) + m_{gas} \cdot \left(h_{e3,gasout} - h_{gex,gasout}\right)}{h_{18} - h_{16}} \quad (5)$$

(vi) Isentropic efficiency of compressor [40]:

$$\varepsilon_{is} = (h_{19s'} - h_{18'})/(h_{19'} - h_{18'}) \quad (6)$$

$$\varepsilon_{is} = 0.815 + 0.022(P_{19'}/P_{18'}) - 0.0041(P_{19'}/P_{18'})^2 + 0.0001(P_{19'}/P_{18'})^3 \quad (7)$$

(vii) COP of CO_2 heat pump cycle:

$$COP_{h,CO_2} = \frac{Q_g}{W_{com}} \quad (8)$$

2. ORC system:

(i) Work output of expander:

$$W_t = m_{R245fa}(h_{13} - h_{14s}) \times \eta_t \times \eta_{gen} = m_{R245fa}(h_{13} - h_{14}) \times \eta_{gen} \quad (9)$$

(ii) Power consumption of pump:

$$W_{pump} = m_{R245fa}(h_{11s} - h_{15})/\eta_{pump} = m_{R245fa}(h_{11} - h_{15}) \quad (10)$$

(iii) Refrigerating effect of evaporator1:

$$Q_{e1} = m_{R245fa}(h_{13} - h_{11}) \quad (11)$$

(v) Heating effect of condenser1:

$$Q_{c1} = m_{R245fa}(h_{14} - h_{15}) \quad (12)$$

(vi) Mass flow of R245fa (ORC cycle):

$$m_{R245fa} = \frac{m_{gas} \cdot (h_{e1,gasin} - h_{e1,gasout})}{h_{13} - h_{11}} \quad (13)$$

(vii) Thermal efficiency of ORC cycle:

$$\eta_{th,orc} = \frac{W_t - W_{pump}}{m_{gas} \cdot (h_{e1,ga\,sin} - h_{e1,gasout})} \quad (14)$$

where η_{pump} is the isentropic efficiency of the working fluid pump, η_t is the isentropic efficiency, η_{gen} is the power generation efficiency (η_{pump} = 0.8, η_t = 0.85, η_{gen} = 1) [41].

3. AHP cycle system:

(i) Refrigerating effect of generator:

$$Q_{ge} = m_4 h_4 + m_{wa} h_7 - m_3 h_3 \quad (15)$$

(ii) Heating effect of absorber:

$$Q_a = m_6 h_6 + m_{wa} h_{10} - m_1 h_1 \quad (16)$$

(iii) Heating effect of condenser2:

$$Q_{c2} = m_{wa}(h_7 - h_8) \quad (17)$$

(iv) Refrigerating effect of evaporator3:

$$Q_{e3} = m_{wa}(h_{10} - h_9) \quad (18)$$

(v) Effect of heat exchanger:

$$Q_{ex} = m_3 h_3 - m_2 h_2 \quad (19)$$

(vi) Bleeding range:

$$\Delta X = x_s - x_w \tag{20}$$

(vii) Circulation ratio:

$$f = \frac{x_s}{x_s - x_w} \tag{21}$$

(viii) Mass flow of refrigerant (water):

$$m_{wa} = \frac{Q_{e3}}{h_{10} - h_9} \tag{22}$$

(ix) Mass flow of strong solution:

$$m_s = (f - 1) \cdot m_{wa} \tag{23}$$

(x) Mass flow of weak solution:

$$m_w = f \cdot m_{wa} \tag{24}$$

(xi) Energy earnings coefficient of AHP system:

$$\Pi_{AHP} = \frac{Q_a + Q_{c2}}{Q_{ge} + Q_{e3}} \tag{25}$$

where, ΔX is the discharge range of the absorption heat pump, %; x_w is the concentration of LiBr weak solution, %; x_s is the concentration of LiBr strong solution, %. To maintain the safe and stable operation of the absorption heat pump, the discharge range is generally between 3% and 5%.

4. OACCHP system:

(i) Heating COP of system:

$$COP_{h,OACCHP} = \frac{Q_{CO_2} + Q_a + Q_{c2}}{W_{com} + W_{pump} - W_t} \tag{26}$$

(ii) Thermal efficiency of flue gas waste heat [42]:

$$\eta_{th,OACCHP} = \frac{Q_{CO_2} + Q_a + Q_{c2} + W_t - W_{pump}}{m_{gas} \cdot \left(h_{e1,ga\sin} - h_{gex,gasout}\right)} \tag{27}$$

(iii) Energy earnings coefficient of system:

$$\Pi_{OACCHP} = \frac{E_{gain}}{E_{pay}} = \frac{Q_{CO_2} + Q_a + Q_{c2} + W_t}{m_{gas} \cdot \left(h_{e1,ga\sin} - h_{gex,gasout}\right) + W_{com} + W_{pump}} \tag{28}$$

2.5. Research Steps

Figure 4 shows the calculation process of various parameters. Firstly, the mass flow and inlet/outlet temperature of the flue gas are set, and then the state parameters of the three subsystems are inputted. Secondly, the corresponding system parameters are obtained through their respective thermodynamic models. Finally, the performance parameters of the OACCHP system are obtained by combining the output parameters of the three subsystems. In addition, as the refrigerant is CO_2 in the CHP cycle, the CHP cycle is a transcritical cycle, and there is an optimal discharge pressure in the system. It is very important to determine the optimal high pressure. This paper adopts the iterative calculation method to determine the optimal performance parameters of the CHP cycle. Firstly, input relevant parameters of CHP cycle and then assume a high pressure range. Secondly, calculate the COP of the system, when the system gets the maximum COP, the corresponding discharge

pressure (P_{dis}) is the optimal pressure (P_{opt}). Finally, output P_{opt} and other performance parameters. All calculation processes are calculated by engineering software EES, and the thermophysical properties of all fluids were obtained by NIST REFPROP9.0.

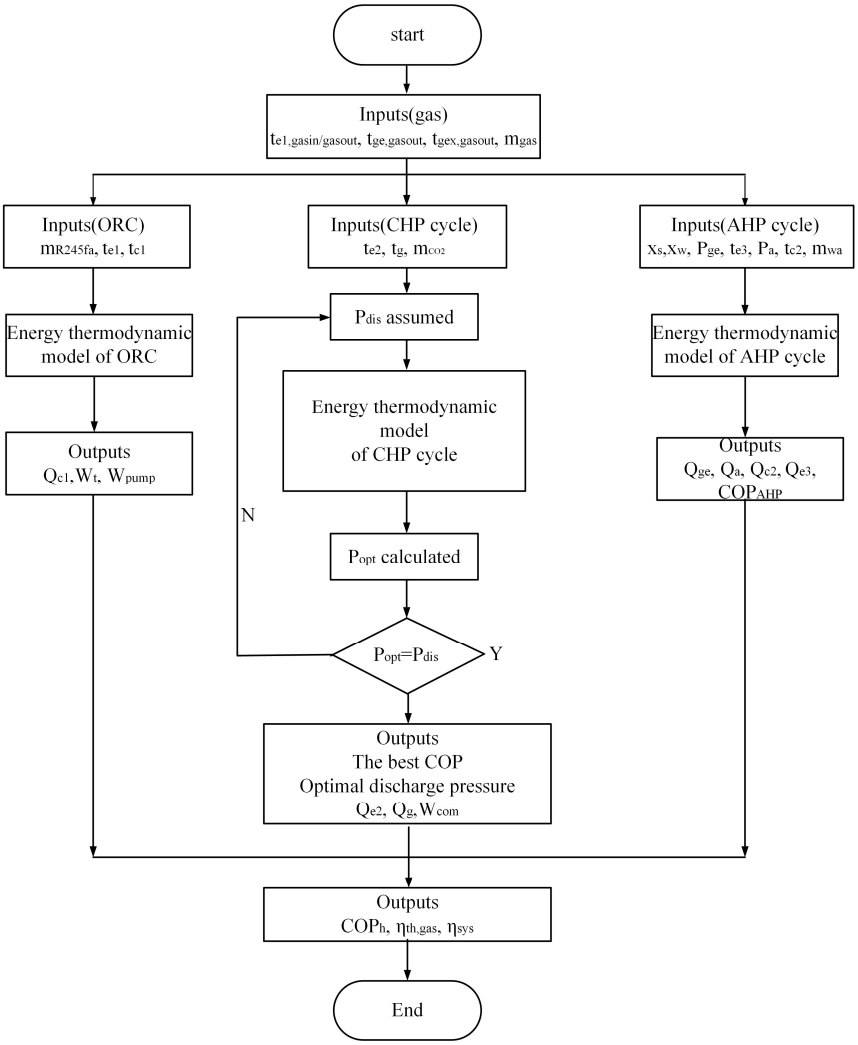

Figure 4. The flow diagram of research steps.

2.6. Simulated Conditions

The working conditions studied in this paper are shown in Table 3, where 'biomass flue gas' is selected as the waste heat source, it includes latent heat and sensible heat [43], and the specific heat distribution curve of biomass flue gas is shown in Figure 5.

Table 3. Simulated operating parameters.

Parameter	OACCHP System
Mass flow of flue gas (m_{gas})/m^3/h	1188
Inlet temperature of flue gas ($t_{e1,gasin}$)/°C	200
Outlet temperature of flue gas ($t_{gex,gasin}$)/°C	30
Temperature of flue gas at the outlet of evaporation1 ($t_{e1,gasout}$)/°C	140–160
Temperature of flue gas at the outlet of generator ($t_{ge,gasout}$)/°C	100
Evaporation temperature in ORC (t_{e1})/°C	120
Condensation temperature in ORC (t_{c1})/°C	30–40
Concentration of strong solution (x_s)/%	64–52
Concentration of weak solution (x_w)/%	$x_s - \Delta x$
Bleeding range Δx/%	3–5
Condensation temperature in AHP (t_{c2})/°C	70–90
Evaporation temperature in AHP (t_{e3})/°C	40–50
Evaporation temperature in CHP (t_{e2})/°C	10–20
Outlet temperature of gas cooler in CHP (t_g)/°C	30–40

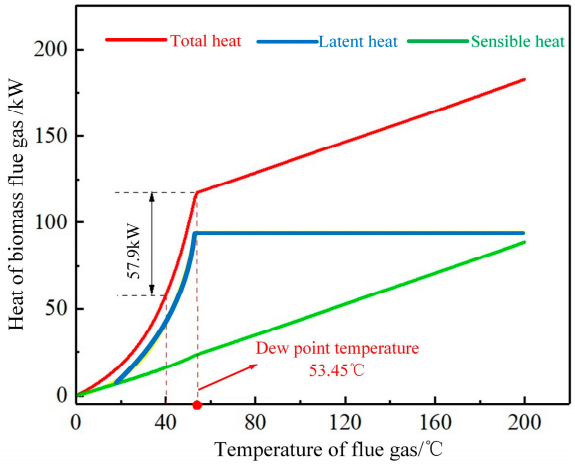

Figure 5. Heat distribution of biomass flue gas.

3. Results and Discussion

3.1. Effect of Different Factors on the System Parameters

3.1.1. Effect of Flue Gas Temperature at evaporator1 Outlet on System Parameters

Figure 6a–d shows the effect of flue gas temperature at evaporator1 outlet on system parameters. It can be seen from Figure 6a that the output work, pump power consumption, net work, and condensing heat in ORC all decrease with the increase in flue gas temperature at evaporator1 outlet. This is because with the increase in flue gas temperature at evaporator1 outlet, the heat absorption of evaporator1 decreases and the mass flow of R245fa decreases, thus resulting in output work, pump power consumption, net work, and condensing heat are reduced. From Figure 6b, it can be seen that in the CHP cycle, the optimal pressure and COP do not change with the increase in flue gas temperature at the evaporator1 outlet, but the compressor power consumption decreases with the increase in flue gas temperature at the evaporator1 outlet. This is because the optimal pressure and COP of the CHP cycle are only related to its own evaporation temperature and the temperature of the gas cooler outlet and they are not affected by external factors. With the decrease in condensing heat in ORC, the mass flow of CO_2 decreases, thus compressor power consumption is reduced. It can be seen from Figure 6c that the heat released by the condenser, the heat absorbed by the evaporator, the heat released by the absorber and the heat absorbed by the generator in the AHP cycle all increase with the increase in the flue gas temperature at evaporator1 outlet. This is because with the increase in flue gas temperature at evaporator1 outlet, the heat absorbed by the generator increases, resulting in the mass

flow of water increases, and the heat absorption/release of each component in the AHP cycle increases. At the same time, as the heat absorption of evaporator3 increases, the flue gas temperature at the outlet of evaporator3 decreases, and the heat transfer of flue gas heat exchanger decreases, further the mass flow of CO_2 in CHP reduces, which also reflects the trend of compressor power consumption in Figure 6b. It can be seen from Figure 6d that with the increase in flue gas temperature at evaporator1 outlet, the heat production of AHP cycle and CHP cycle shows an opposite trend, but the total heat production of the system decreases with the increase in flue gas temperature at evaporator1 outlet, which is also the same as the change trend of heat production in the CHP cycle, indicating that the heat production of CHP cycle plays a dominant role at this time. In addition, the heat production of CHP cycle is significantly higher than that of AHP cycle.

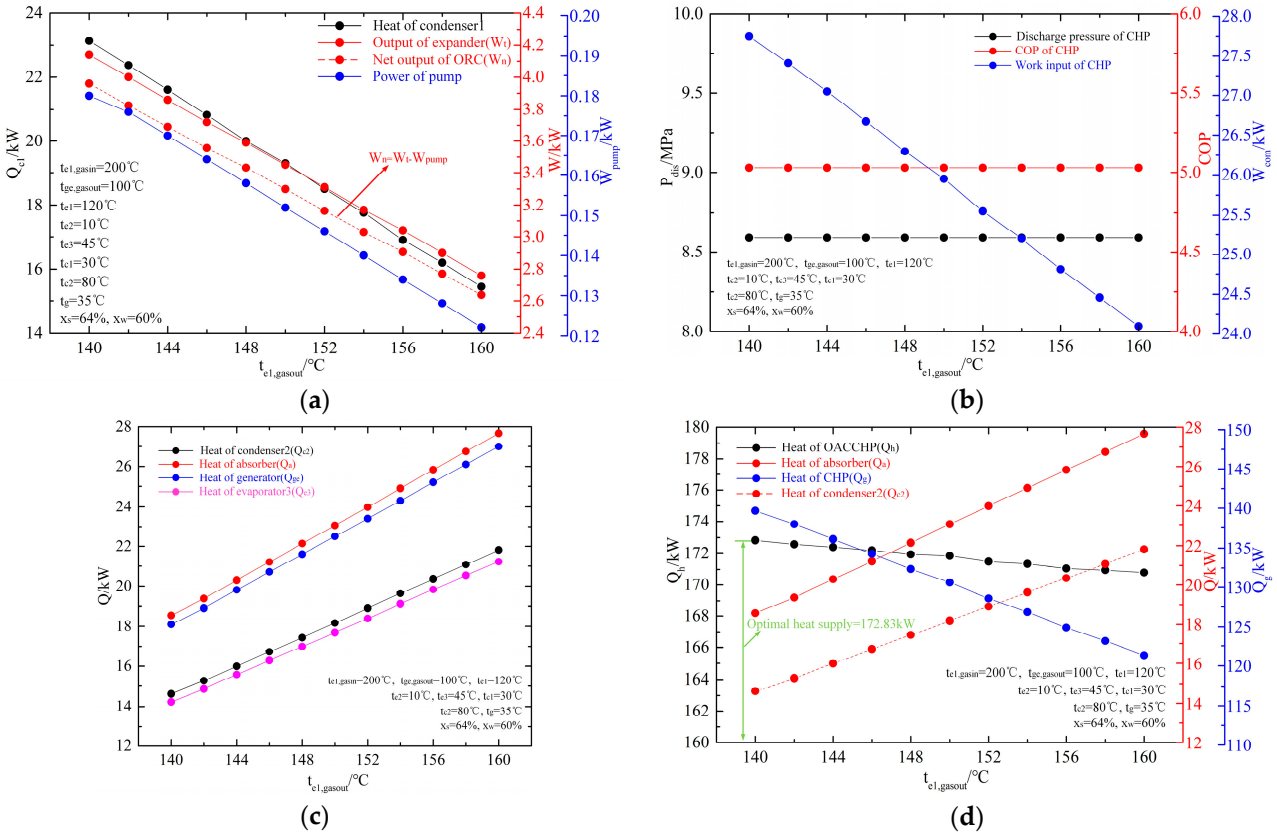

Figure 6. Effect of flue gas temperature at evaporator1 outlet on system parameters ($t_{e1,gasin}$ = 200 °C, $t_{ge,gasout}$ = 100 °C, t_{e1} = 120 °C, t_{e2} = 10 °C, t_{e3} = 45 °C, t_{c1} = 30 °C, t_{c2} = 80 °C, t_g = 35 °C, x_s = 64%, x_w = 60%). (**a**) Q_{cl} changes with $t_{e1,gasout}$. (**b**) Performance changes with $t_{e1,gasout}$. (**c**) Q changes with $t_{e1,gasout}$. (**d**) Heat performance changes with $t_{e1,gasout}$.

In the given range of flue gas temperature at evaporator1 outlet, the heat production of condenser1, gas cooler, and total are reduced by 33.23%, 13.13%, and 1.17%, respectively. The heat transfer increase in condenser3, absorber, generator, and evaporator3 is basically the same, which is about 49.17%. Output work, net work, and pump power consumption are all reduced by about 33.33%, and compressor power consumption is reduced by 13.15%.

In addition, for different application scenarios, the net output work and total heat production of the system have the same change trend under the effect of the flue gas temperature at evaporator1 outlet, so the flue gas temperature at evaporator1 outlet should be appropriately reduced no matter in the scenario dominated by power generation or heating.

3.1.2. Effect of Condensing Temperature of ORC on System Parameters

Figure 7a–c shows the effect of condensing temperature of ORC on system parameters. It can be seen from Figure 7a that both output work and net work in ORC decrease with the increase in condensing temperature of ORC, while heat release of condenser1 and power consumption of the pump increase with the increase in condensing temperature of ORC. This is because the increase in condensing temperature reduces the enthalpy difference between import and export of evaporator1, while the heat absorption of evaporator1 remains unchanged, resulting in the mass flow of R245fa increases. At the same time, the unit output work of the expander decreases, and the influence of the unit output work of the expander is greater than that of the mass flow, which reduces the output work. It can be seen from Figure 7b that in CHP cycle, the variation trend of compressor power consumption is consistent with that of condenser heat release in ORC, for the same reasons as above. Since the condensing temperature in ORC does not directly affect the AHP cycle, the heat absorption/release of each component in the AHP cycle remains unchanged. As can be seen from Figure 7c, as the condensing temperature of ORC increases, both the heat release in CHP and the total heat production increase.

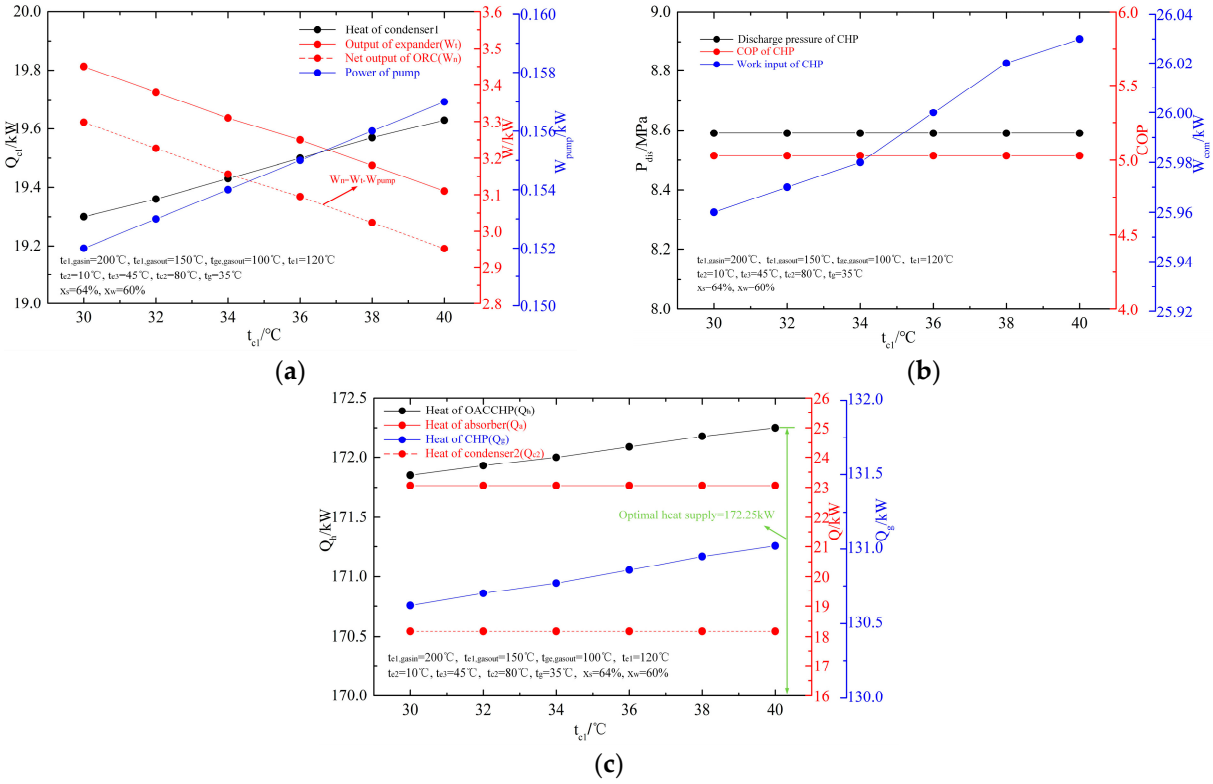

Figure 7. Effect of condensing temperature of ORC on system parameters ($t_{e1,gasin}$ = 200 °C, $t_{ge,gasout}$ = 100 °C, t_{e1} = 120 °C, t_{e2} = 10 °C, t_{e3} = 45 °C, $t_{e1,gasout}$ = 150 °C, t_{c2} = 80 °C, t_g = 35 °C, x_s = 64%, x_w = 60%). (**a**) Q_{cl} changes with t_{c1}. (**b**) Performance changes with t_{c1}. (**c**) Heat performance changes with t_{c1}.

In the given range of condensing temperature of ORC, the heat production of condenser1, gas cooler, and total are increased by 1.7%, 0.31%, and 0.23%, respectively. Output power and net power are decreased by 9.85% and 10.33%, respectively. Pump power consumption and compressor power consumption are increased by 3.28% and 0.26%, respectively. It can be seen that the condensing temperature of ORC has little effect on the system parameters.

In addition, for different application scenarios, the net output work and total heat production of the system have opposite trends under the effect of the condensing temperature

of ORC. Therefore, the condensing temperature of ORC should be appropriately reduced for the scenario mainly based on power generation, while the condensing temperature of ORC should be appropriately increased for the scenario mainly based on heating.

3.1.3. Effect of Concentration of LiBr Strong Solution on System Parameters

Figure 8a–c shows the effect of the concentration of LiBr strong solution on system parameters. As can be seen from Figure 8a, the compressor power consumption increases with the increase in LiBr strong solution concentration. This is because when the concentration of LiBr strong solution increases, the heat absorption of the generator remains unchanged, resulting in the mass flow of water decreasing in AHP, therefore, the heat absorption of evaporator3 decreases. At the same time, the flue gas temperature at evaporator3 outlet increases, and the mass flow of CO_2 increases, resulting in compressor power consumption increases. As can be seen from Figure 8b, the heat production of the gas cooler and the AHP system shows an opposite trend, but the heat production of the gas cooler still dominates, so the heat production of both the total and gas cooler also increases with the increase in LiBr strong solution concentration. At the same time, by combining Figure 8b,c, it can be found that the decrease in mass flow of water directly leads to the decrease in heat transfer in condenser2 and evaporator3. While the heat release of the absorber decreases due to combining the change in mass flow of water and LiBr strong solution concentration but the overall situation remains the same. In addition, the change in LiBr concentration has no effect on ORC parameters.

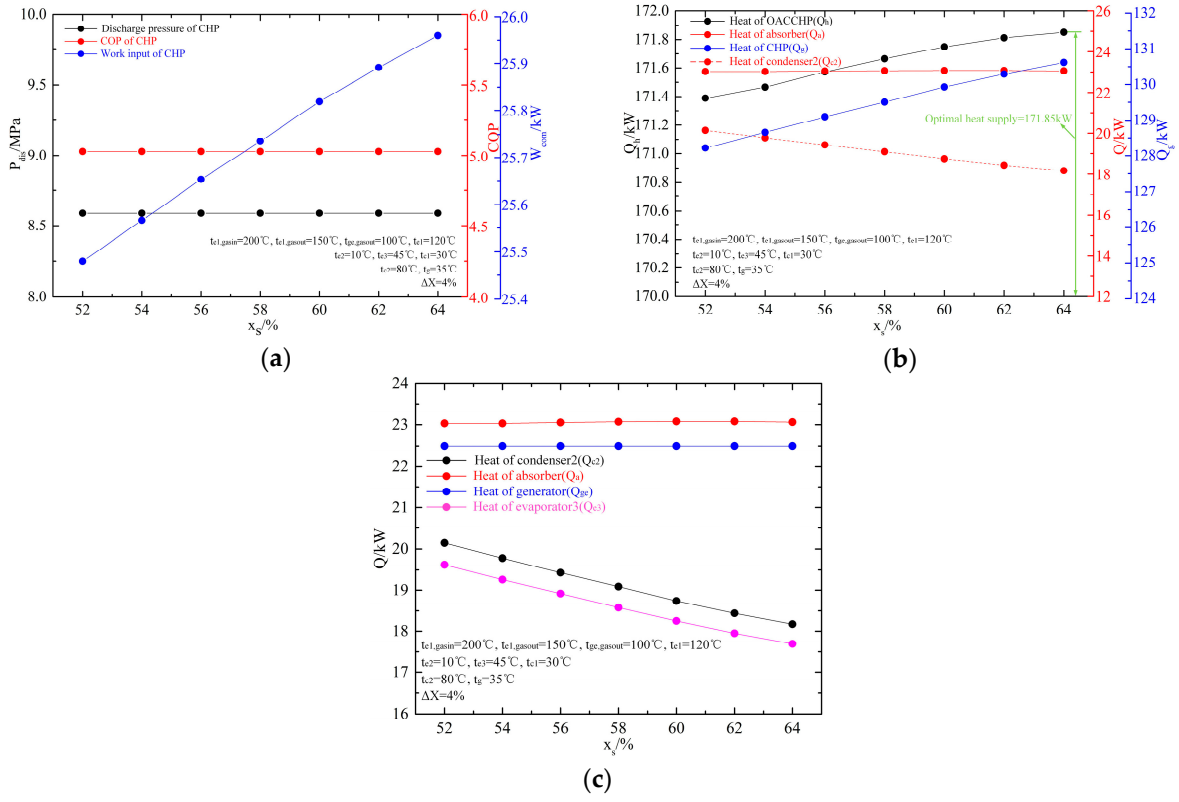

Figure 8. Effect of concentration of LiBr strong solution on system parameters ($t_{e1,gasin}$ = 200 °C, $t_{ge,gasout}$ = 100°C, t_{e1} = 120 °C, t_{e2} = 10 °C, t_{e3} = 45 °C, $t_{e1,gasout}$ = 150 °C, t_{c1} = 30 °C, t_{c2} = 80 °C, t_g = 35 °C, ΔX = 4%). (**a**) Performance changes with x_s. (**b**) Heat performance changes with x_s. (**c**) Q changes with x_s.

In the given range of LiBr strong solution concentration, the heat production of the gas cooler and total is increased by 1.87% and 0.27%, respectively. Compressor power consumption is increased by 1.92%. The heat transfer of condenser3 and evaporator3 is reduced by 9.78% and 9.83%, respectively.

In addition, for different application scenarios, the net work output of the system remains the same under the effect of the concentration of LiBr strong solution, while the total heat production of the system changes. Therefore, the concentration of LiBr strong solution should be appropriately increased for both the power generation and heating scenarios.

3.1.4. Effect of Bleeding Range on System Parameters

Figure 9a–c shows the effect of bleeding range on system parameters. Combined with Figure 9a–c, it can be seen that the heat transfer of condenser2 and evaporator3 increases with the increase in bleeding range, but the increase is small. This is also because the increase in bleeding range will increase the mass flow of water in AHP, so the heat transfer of condenser2 and evaporator3 will increase. Similarly, the decrease in heat transfer of the flue gas heat exchanger and the mass flow of CO_2 reduces the compressor work, the heat discharge, and the total heat production of the gas cooler.

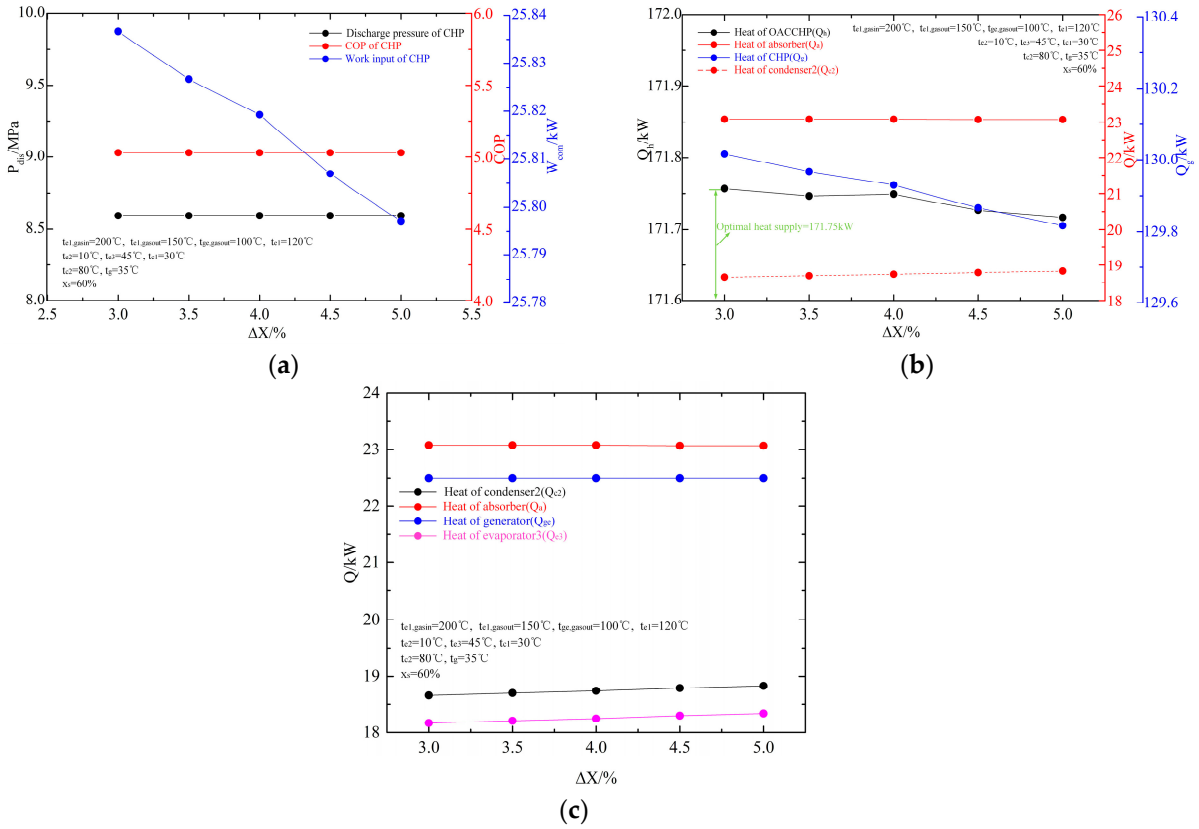

Figure 9. Effect of bleed range on system parameters ($t_{e1,gasin}$ = 200 °C, $t_{ge,gasout}$ = 100 °C, t_{e1} = 120 °C, t_{e2} = 10 °C, t_{e3} = 45 °C, $t_{e1,gasout}$ = 150 °C, t_{c1} = 30 °C, t_{c2} = 80 °C, t_g = 35 °C, x_s = 60%). (**a**) Performance changes with Δx. (**b**) Heat performance changes with Δx. (**c**) Q changes with Δx.

In a given bleeding range, the heat production of the gas cooler and total is reduced by 0.15% and 0.02%, respectively. Compressor power consumption is reduced by 0.15%. The heat transfer of condenser3 and evaporator3 is increased by 0.91% and 0.93%, respectively. It can be seen that the effect of the bleeding range on the system parameters is very small, so the effect of this factor on the system can be ignored.

3.1.5. Effect of Condensing Temperature of AHP on System Parameters

Figure 10a–c shows the effect of condensing temperature of AHP on system parameters. Combined with Figure 10a–c, it can be seen that with the increase in condensing temperature of AHP, the saturation pressure in condenser2 increases, the mass flow water increases, the heat release of the absorber increases, and the unit latent heat capacity of

water decreases, and at this time, the unit latent heat capacity of water plays a dominant role, so the heat release of condenser2 decreases. At the same time, as the condensing temperature of AHP increases, the unit enthalpy value after throttling increases (state point 9), so the unit heat absorption of evaporator3 decreases, and the effect of this factor is stronger than that of mass flow of water, so the heat absorption of evaporator3 decreases. In addition, due to the decrease in heat absorption in evaporator3, the heat transfer of the flue gas heat exchanger increases, further increasing the mass flow of CO_2, resulting in the increase in compressor power consumption, gas cooler heat release, and total heat production.

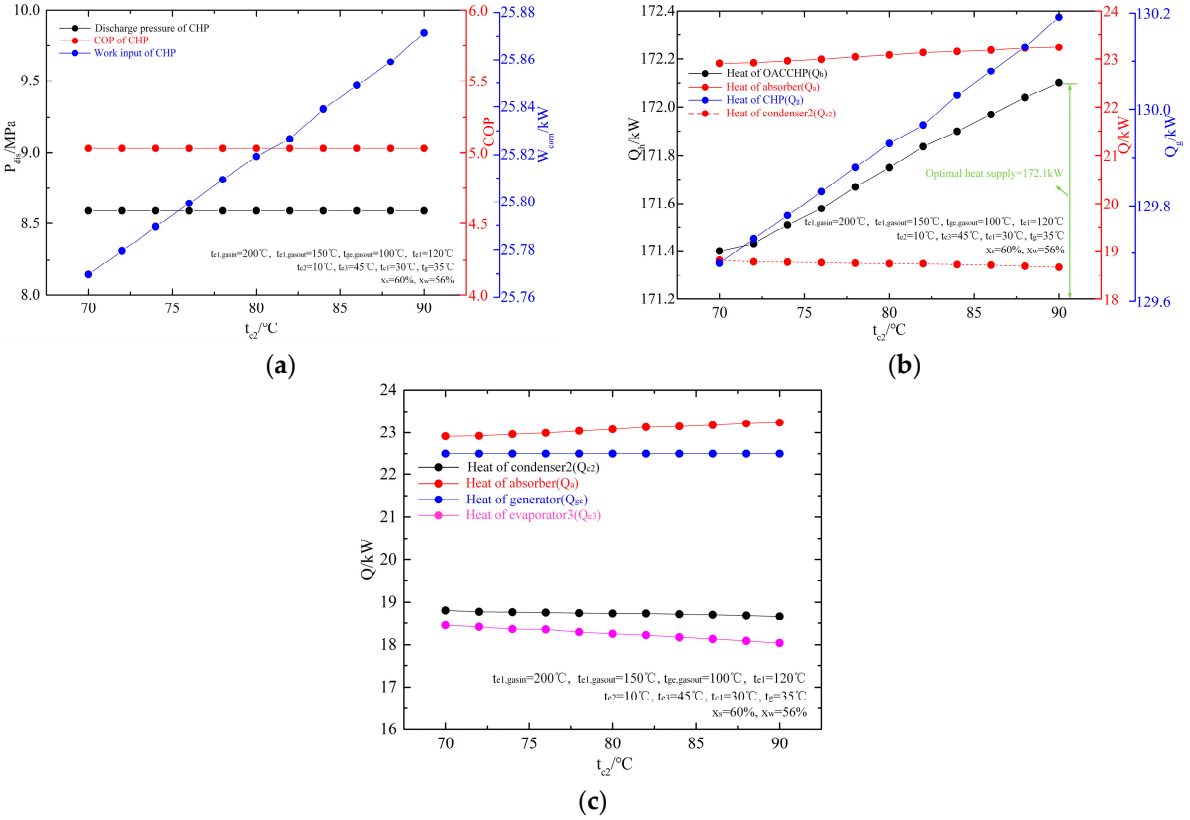

Figure 10. Effect of condensing temperature of AHP on system parameters ($t_{e1,gasin}$ = 200 °C, $t_{ge,gasout}$ = 100 °C, t_{e1} = 120 °C, t_{e2} = 10 °C, t_{e3} = 45 °C, $t_{e1,gasout}$ = 150 °C, t_{c1} = 30 °C, t_g = 35 °C, x_s = 60%, x_w = 56%). (**a**) Performance changes with t_{c2}. (**b**) Heat performance changes with t_{c2}. (**c**) Q changes with t_{c2}.

In a given range of AHP condensing temperature, the heat production of gas cooler and total is increased by 0.41% and 0.4%, respectively. Compressor power consumption is increased by 0.43%. The heat transfer of condenser3 and evaporator3 is reduced by 0.74% and 1.44%, respectively. The heat release of the absorber is increased by 2.22%.

In addition, the condensing temperature of AHP should be appropriately increased for both power-generating and heating scenarios.

3.1.6. Effect of Evaporation Temperature of AHP on System Parameters

Figure 11a–c shows the effect of the evaporation temperature of AHP on system parameters. Combined with Figure 11a–c, it can be seen that with the increase in evaporation temperature of AHP, heat absorption of evaporator3 increases. This is because the condensing temperature, condensing pressure, and heat absorption of the generator are unchanged at this time, so the mass flow of water is unchanged, and the enthalpy value of state point9 is unchanged. While the enthalpy value of state point 10 is increased, the heat absorption of evaporator3 is increased. The heat release of the absorber is reduced because of the change in enthalpy of water and LiBr solution.

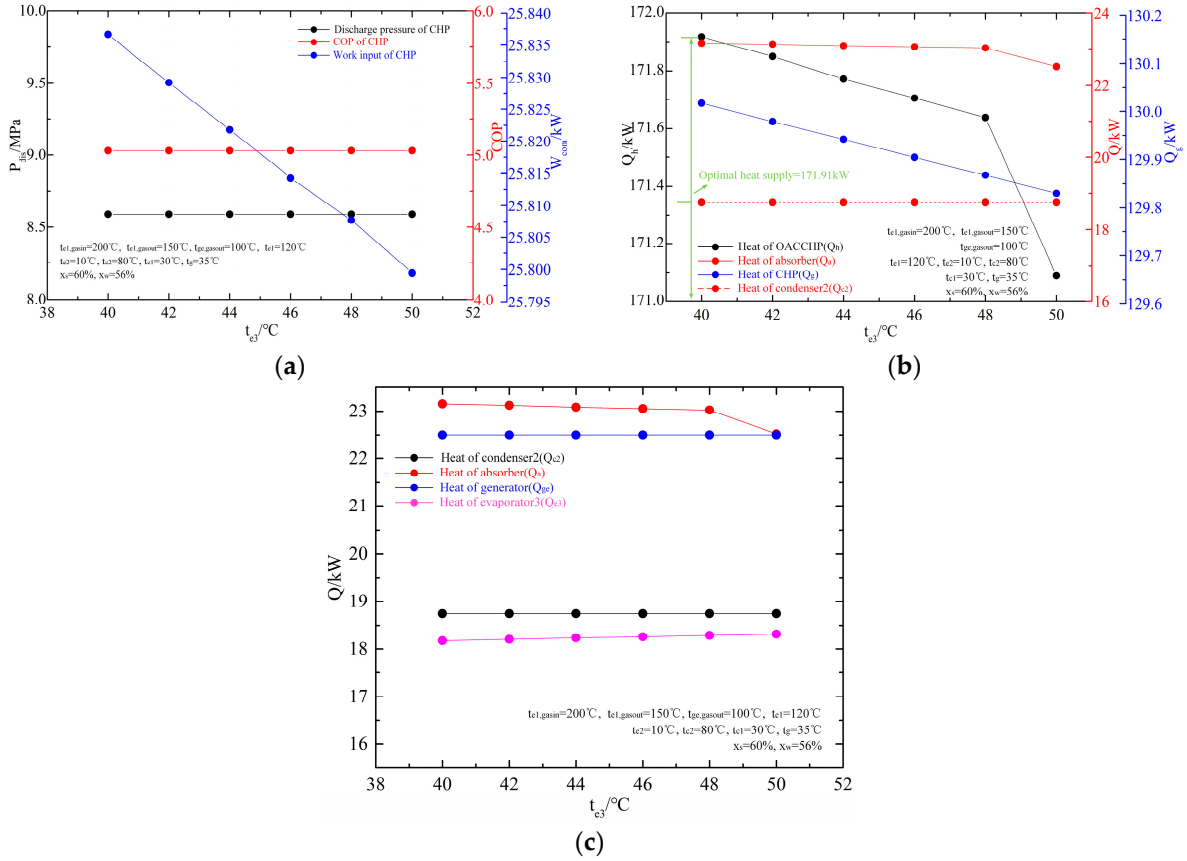

Figure 11. Effect of evaporation temperature of AHP on system parameters ($t_{e1,gasin}$ = 200 °C, $t_{ge,gasout}$ = 100 °C, t_{e1} = 120 °C, t_{e2} = 10 °C, $t_{e1,gasout}$ = 150 °C, t_{c1} = 30 °C, t_{c2} = 80 °C, t_g = 35°C, x_s = 60%, x_w = 56%). (**a**) Performance changes with t_{e3}. (**b**) Heat performance changes with t_{e3}. (**c**) Q changes with t_{e3}.

In a given range of AHP evaporation temperature, the heat production of the gas cooler and total is reduced by 0.15% and 0.48%, respectively. Compressor power consumption is reduced by 0.15%. The heat absorption of evaporator3 is increased by 0.77%. The heat release of absorber is reduced by 2.76%.

In addition, the evaporation temperature of AHP should be appropriately reduced for both power generation and heating scenarios.

3.1.7. Effect of Evaporation Temperature of CHP on System Parameters

Figure 12a,b shows the effect of the evaporation temperature of CHP on the system parameters. It can be seen from Figure 12a,b that with the increase in evaporation temperature of CHP, the optimal pressure of the system decreases, which reduces the compression ratio and unit power consumption. Meanwhile, the mass flow of CO_2 remains unchanged, so the power consumption of the system decreases. At the same time, the decrease in discharge pressure decreases the discharge temperature, so the heat production of CHP is decreased, and the heat production of the total is also decreased. In addition, as the reduction of compressor power consumption is greater than that of heat production, the COP of the system increases.

In a given range of CHP evaporation temperature, the heat production of the gas cooler and total is reduced by 7.56% and 5.74%, respectively. The compressor power consumption is decreased by 38.03%, the optimal pressure is decreased by 1.86%, and COP is increased by 49.1%. At the same time, the parameter change in CHP does not affect ORC and AHP.

In addition, the evaporation temperature of CHP should be reduced appropriately for both power-generating and heating scenarios.

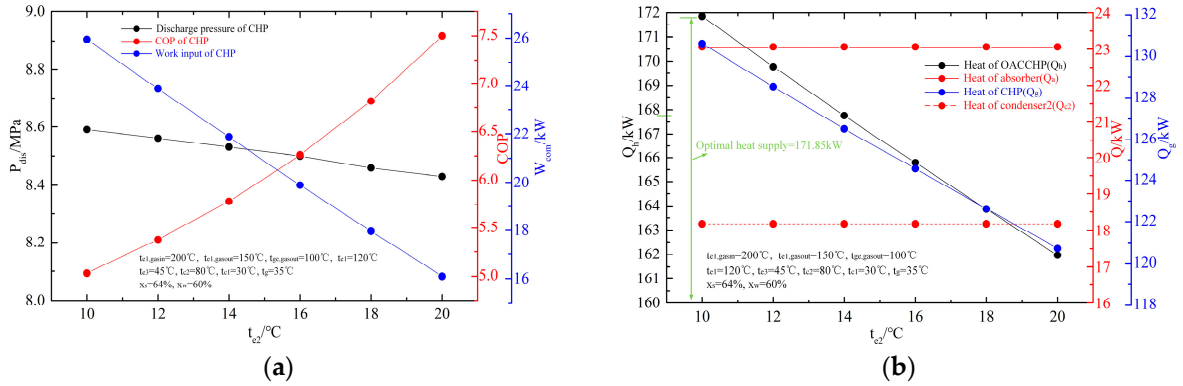

Figure 12. Effect of evaporation temperature of CHP on system parameters ($t_{e1,gasin}$ = 200 °C, $t_{ge,gasout}$ = 100 °C, t_{e1} = 120 °C, t_{e3} = 45 °C, $t_{e1,gasout}$ = 150 °C, t_{c1} = 30 °C, t_{c2} = 80 °C, t_g = 35 °C, x_s = 64%, x_w = 60%). (**a**) Performance changes with t_{e2}. (**b**) Heat performance changes with t_{e2}.

3.1.8. Effect of Outlet Temperature of Gas Cooler on System Parameters

Figure 13a,b shows the effect of the outlet temperature of the gas cooler on system parameters. It can be seen from Figure 13a,b that with the increase in the outlet temperature of the gas cooler, the optimal pressure of the system increases, which increases the compression ratio and unit power consumption. The mass flow of CO_2 remains unchanged, so the power consumption of the system increases. At the same time, the discharge temperature increases, so the heat production of CHP increases, and the heat production of the total also increases. In addition, the COP of the system decreases because the increase in compressor power consumption is greater than that of heat production.

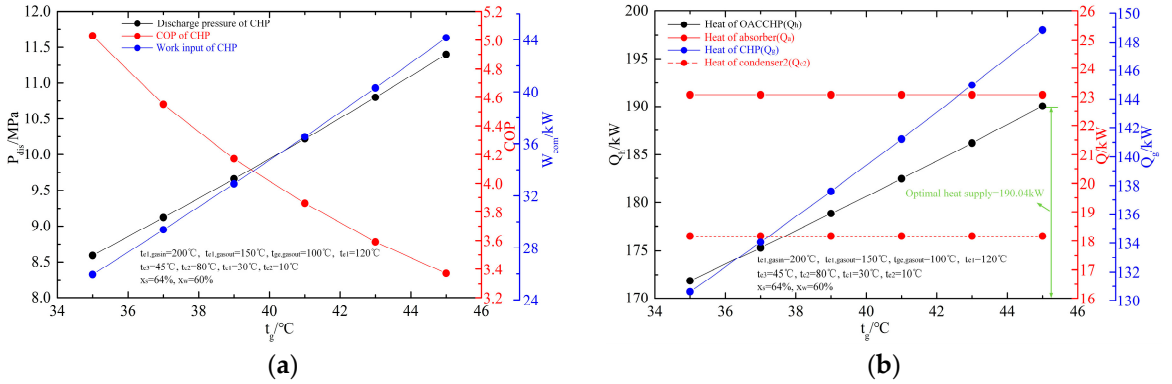

Figure 13. Effect of outlet temperature of gas cooler on system parameters ($t_{e1,gasin}$ = 200 °C, $t_{ge,gasout}$ = 100 °C, t_{e1} = 120 °C, t_{e2} = 10 °C, t_{e3} = 45 °C, $t_{e1,gasout}$ = 150 °C, t_{c1} = 30 °C, t_{c2} = 80 °C, x_s = 64%, x_w = 60%). (**a**) Performance changes with t_g. (**b**) Heat performance changes with t_g.

In the given range of the outlet temperature of the gas cooler, the heat production of the gas cooler and total is increased by 13.92% and 10.58%, respectively. The compressor power consumption is increased by 70.13%, the optimal pressure is increased by 32.7%, and COP is decreased by 33%.

In addition, no matter if the scenario is mainly based on power generation or heating, the outlet temperature of the gas cooler should be properly reduced, that is, some heat production is lost to ensure that the system pressure is lower so the system operation is safer and more stable.

According to the above research, it is found that the flue gas temperature at evaporator1 outlet and the factors from CHP have a greater impact on the power generation and heat generation of the OACCHP system, while the factors from AHP have a smaller impact on the power generation and heat generation of the system. In addition, the optimal working

conditions for the scenario or objectives dominated by power generation (Power) and the scenario dominated by heat production (Heat) are shown in Table 4.

Table 4. Optimal operating conditions of production.

Objectives	$t_{e1,gasin}$/°C	$t_{ge,gasout}$/°C	t_{e1}/°C	t_{e2}/°C	t_{e3}/°C	$t_{e1,gasout}$/°C	t_{c1}/°C	t_{c2}/°C	t_g/°C	x_s/%	x_w/%
Power	200	100	120	20	50	140	30	70	35	52	48
Heat	200	100	120	10	40	140	40	90	35	64	60

3.2. Effect of Different Factors on System Performance Indexes

3.2.1. Effect of Flue Gas Temperature at evaporator1 Outlet on System Performance Indexes

Figure 14 shows the effect of flue gas temperature at evaporator1 outlet on the performance indexes of different systems. It can be seen that the thermal efficiency of the OACCHP system is significantly higher than that of the single ORC system, and the COP and energy earning rate of the OACCHP system are also improved to a certain extent compared with the single CHP system and the single AHP system. When the flue gas temperature at evaporator1 outlet increases, the thermal efficiency and energy earning rate of the OACCHP system are basically unchanged, while the COP increases significantly. Moreover, the COP of the OACCHP system is increased by 0.48% on average with the increase of one degree of flue gas temperature at evaporator1 outlet.

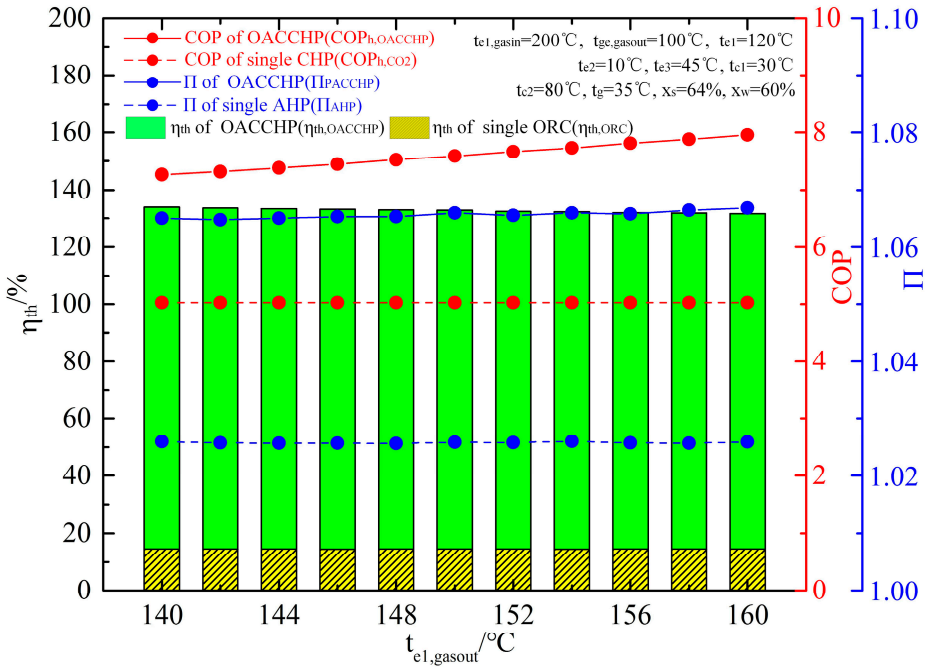

Figure 14. Effect of flue gas temperature at evaporator1 outlet on system performance indexes ($t_{e1,gasin}$ = 200 °C, $t_{ge,gasout}$ = 100 °C, t_{e1} = 120 °C, t_{e2} = 10 °C, t_{e3} = 45 °C, t_{c1} = 30 °C, t_{c2} = 80 °C, t_g = 35 °C, x_s = 64%, x_w = 60%).

In the given range of flue gas temperature at evaporator1 outlet, compared with the single ORC system, the single CHP system, and the single AHP system, the thermal efficiency, COP, and energy earning rate of the OACCHP system are increased by 710.14%, 50.89%, and 3.9%, respectively.

In addition, from the perspective of efficiency and COP, the flue gas temperature at evaporator1 outlet should be appropriately increased for different application scenarios.

3.2.2. Effect of Condensing Temperature of ORC on System Performance Indexes

Figure 15 shows the effect of the condensing temperature of ORC on the performance indexes of different systems. It can be seen that the COP of the OACCHP decreases with the increase in ORC condensation temperature, and the COP of the OACCHP system is decreased by 0.15% on average with the increase of one degree of ORC condensation temperature. At the same time, other performance indexes of the system are basically unchanged.

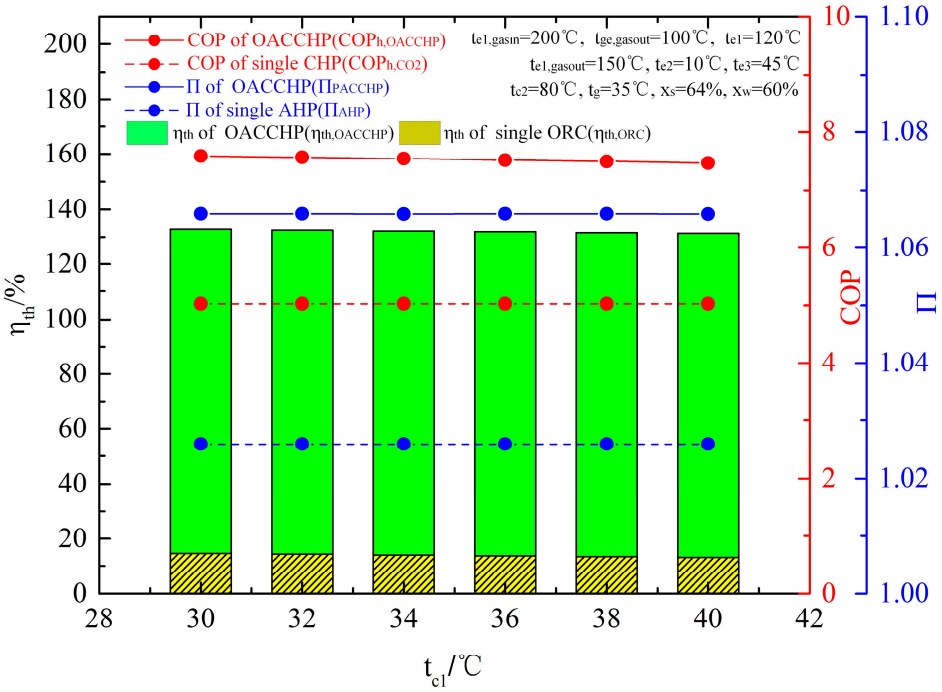

Figure 15. Effect of condensing temperature of ORC on system performance indexes ($t_{e1,gasin}$ = 200 °C, $t_{ge,gasout}$ = 100 °C, t_{e1} = 120 °C, t_{e2} = 10 °C, t_{e3} = 45 °C, $t_{e1,gasout}$ = 150 °C, t_{c2} = 80 °C, t_g = 35 °C, x_s = 64%, x_w = 60%).

In the given range of flue gas temperature at evaporator1 outlet, compared with the single ORC system, the single CHP system, and the single AHP system, the thermal efficiency, COP, and energy earning rate of the OACCHP system are increased by 755.49%, 49.5%, and 5.8%, respectively.

In addition, from the perspective of efficiency and COP, the condensation temperature of ORC should be appropriately reduced for different application scenarios.

3.2.3. Effect of Concentration of LiBr Strong Solution on System Performance Indexes

Figure 16 shows the effect of LiBr strong solution concentration on the performance indexes of different systems. It can be seen that the COP of the OACCHP decreases with the increase in LiBr strong solution concentration, and the COP of the OACCHP system is decreased by 1.16% on average with every 1% increase in LiBr strong solution concentration. At the same time, other performance indexes of the OACCHP system are basically unchanged.

In a given range of LiBr strong solution concentration, compared with the single ORC system, the single CHP system, and the single AHP system, the thermal efficiency, COP, and energy earning rate of the OACCHP system are increased by 709.25%, 52.08%, and 3.92%, respectively.

In addition, from the perspective of efficiency and COP, the concentration of LiBr strong solution should be appropriately reduced for different application scenarios.

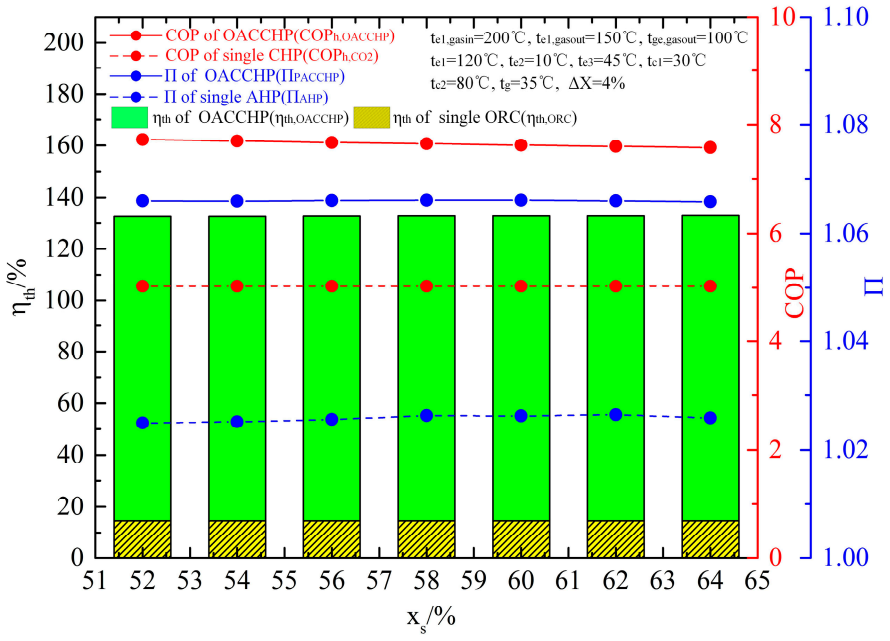

Figure 16. Effect of concentration of LiBr strong solution on system performance indexes ($t_{e1,gasin}$ = 200 °C, $t_{ge,gasout}$ = 100 °C, t_{e1} = 120 °C, t_{e2} = 10 °C, t_{e3} = 45 °C, $t_{e1,gasout}$ = 150 °C, t_{c1} = 30 °C, t_{c2} = 80 °C, t_g = 35°C, ΔX = 4%).

3.2.4. Effect of Bleeding Range on System Performance Indexes

Figure 17 shows the effect of the bleeding range on the performance indexes of different systems. It can be seen that the performance indexes of the OACCHP system are basically unchanged. This also corresponds to the conclusion in Figure 9, which again shows that the effect of bleeding range can be ignored.

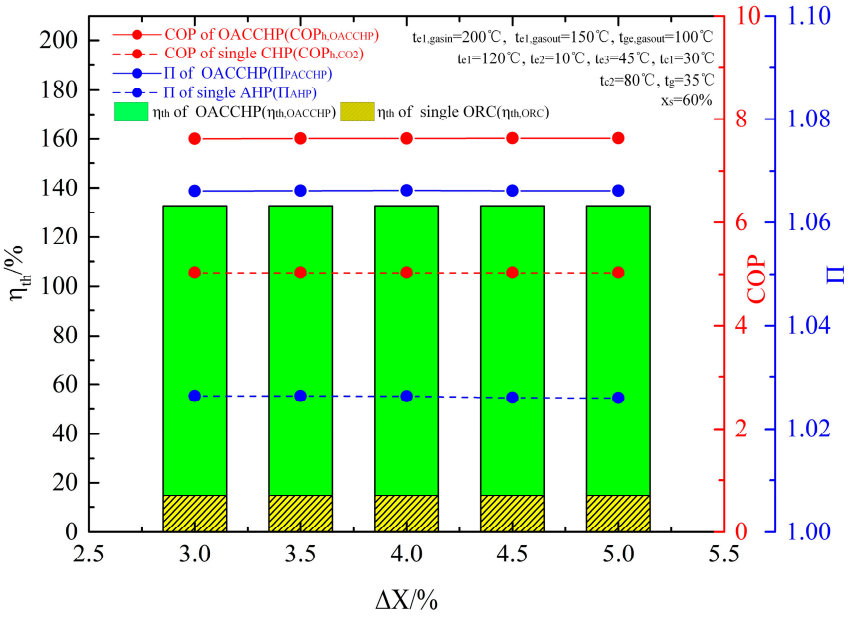

Figure 17. Effect of bleeding range on system performance indexes ($t_{e1,gasin}$ = 200 °C, $t_{ge,gasout}$ = 100 °C, t_{e1} = 120 °C, t_{e2} = 10 °C, t_{e3} = 45 °C, $t_{e1,gasout}$ = 150 °C, t_{c1} = 30 °C, t_{c2} = 80 °C, t_g = 35 °C, x_s = 60%).

In a given bleeding range, compared with the single ORC system, the single CHP system, and the single AHP system, the thermal efficiency, COP, and energy earning rate of the OACCHP system are increased by 709.73%, 51.49%, and 3.88%, respectively.

3.2.5. Effect of Condensing Temperature of AHP on System Performance Indexes

Figure 18 shows the effect of the condensation temperature of AHP on the performance indexes of different systems. It can be seen that the condensation temperature of AHP has little effect on the energy earning rate of the OACCHP system, and every 1 °C increase in the condensation temperature of AHP, the energy earning rate of the OACCHP system is increased by 0.014% on average.

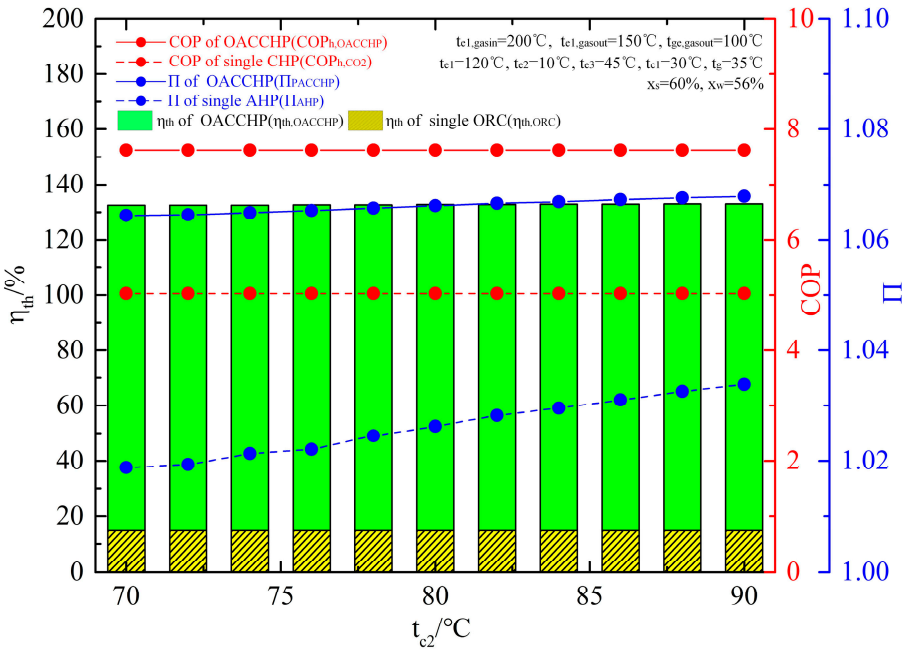

Figure 18. Effect of condensing temperature of AHP on system performance indexes ($t_{e1,gasin}$ = 200 °C, $t_{ge,gasout}$ = 100 °C, t_{e1} = 120 °C, t_{e2} = 10 °C, t_{e3} = 45 °C, $t_{e1,gasout}$ = 150 °C, t_{c1} = 30 °C, t_g = 35 °C, x_s = 60%, x_w = 56%).

In the given range of AHP condensation temperature, compared with the single ORC system, the single CHP system, and the single AHP system, the thermal efficiency, COP, and energy earning rate of the OACCHP system are increased by 709.73%, 51.49%, and 3.88%, respectively.

3.2.6. Effect of Evaporation Temperature of AHP on System Performance Indexes

Figure 19 shows the effect of AHP evaporation temperature on the performance indexes of different systems. It can be seen that the effect of AHP evaporation temperature on the energy earning rate of the OACCHP system is also small, and every 1 °C increase in AHP evaporation temperature, the energy earning rate of the OACCHP system is decreased by 0.042% on average.

In the given range of AHP evaporation temperature, compared with the single ORC system, the single CHP system, and the single AHP system, the thermal efficiency, COP, and energy earning rate of the OACCHP system are increased by 708.97%, 51.49%, and 4%.

3.2.7. Effect of Evaporation Temperature of CHP on System Performance Indexes

Figure 20 shows the effect of CHP evaporation temperature on the performance indexes of different systems. It can be seen that the evaporation temperature of CHP has a great effect on the COP of the OACCHP system, and every 1 °C increase in CHP evaporation temperature, the COP of the OACCHP system is increased by 6.72% on average. The energy earning rate of the OACCHP system decreases slightly with the increase in CHP evaporation temperature.

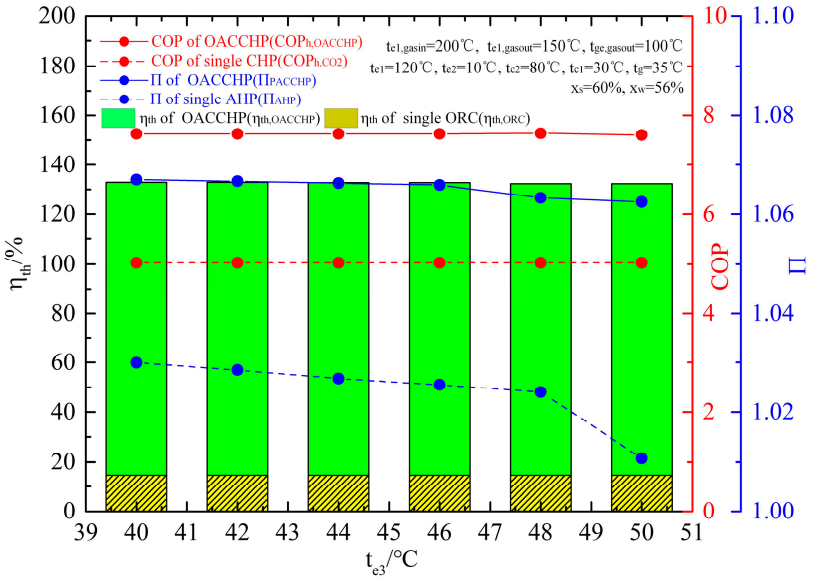

Figure 19. Effect of evaporation temperature of AHP on system performance indexes ($t_{e1,gasin}$ = 200 °C, $t_{ge,gasout}$ = 100 °C, t_{e1} = 120 °C, t_{e2} = 10 °C, $t_{e1,gasout}$ = 150 °C, t_{c1} = 30 °C, t_{c2} = 80 °C, t_g = 35 °C, x_s = 60%, x_w = 56%).

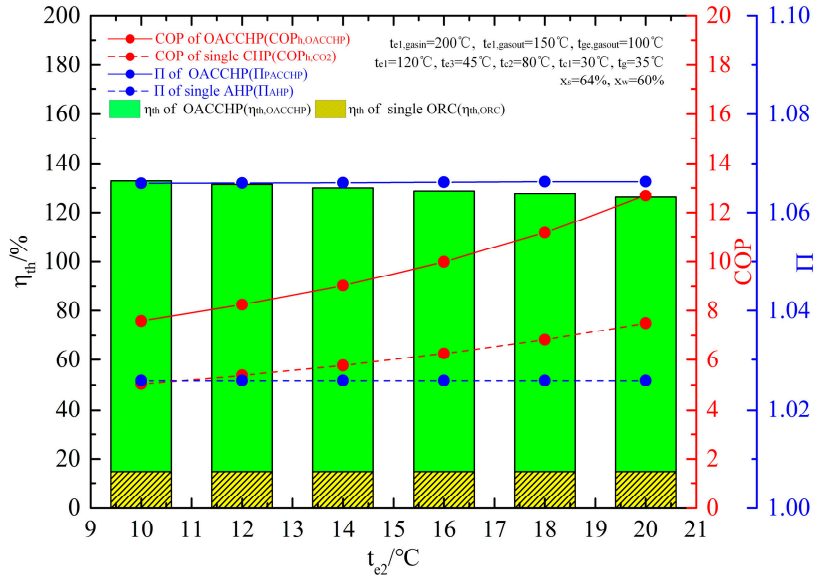

Figure 20. Effect of evaporation temperature of CHP on system performance indexes ($t_{e1,gasin}$ = 200 °C, $t_{ge,gasout}$ = 100 °C, t_{e1} = 120 °C, t_{e3} = 45 °C, $t_{e1,gasout}$ = 150 °C, t_{c1} = 30 °C, t_{c2} = 80 °C, t_g = 35 °C, x_s = 64%, x_w = 60%).

In the given range of CHP evaporation temperature, compared with the single ORC system, the single CHP system, and the single AHP system, the thermal efficiency, COP and energy earning rate of the OACCHP system are increased by 687.05%, 59.8%, and 3.92%.

3.2.8. Effect of Outlet Temperature of Gas Cooler on System Performance Indexes

Figure 21 shows the effect of the outlet temperature of the gas cooler on the performance indexes of different systems. It can be seen that the outlet temperature of the gas cooler also has a great effect on the COP of OACCHP, and every 1 °C increase in the outlet temperature of the gas cooler, the COP of the OACCHP system is increased by 3.86% on

average. Meanwhile, the energy earning rate of the OACCHP system increases slightly with the increase in the outlet temperature of the gas cooler.

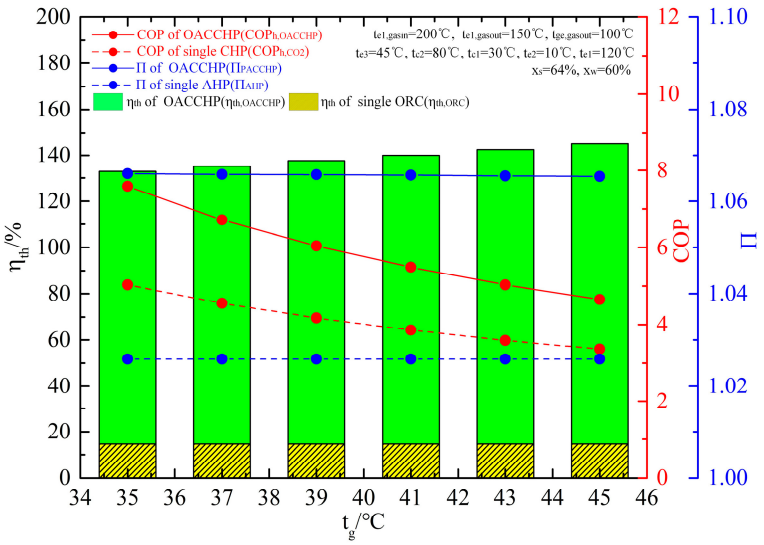

Figure 21. Effect of outlet temperature of gas cooler on system performance indexes ($t_{e1,gasin}$ = 200 °C, $t_{ge,gasout}$ = 100 °C, t_{e1} = 120 °C, t_{e2} = 10 °C, t_{e3} = 45 °C, $t_{e1,gasout}$ = 150 °C, t_{c1} = 30 °C, t_{c2} = 80 °C, x_s = 64%, x_w = 60%).

In the given range of outlet temperature of gas cooler, compared with the single ORC system, the single CHP system, and the single AHP system, the thermal efficiency, COP, and energy earning rate of the OACCHP system are increased by 751.47%, 44.52%, and 3.87%.

According to the above research, it is found that the flue gas temperature at evaporator1 outlet and the factors from CHP have a greater influence on the performance indexes of the OACCHP system, while other factors have a smaller influence on the performance indexes of the OACCHP system. In addition, for scenarios or objectives dominated by different performance indexes, the optimal working conditions are shown in Table 5.

Table 5. Optimal operating conditions of indexes.

Objectives	$t_{e1,gasin}$/°C	$t_{ge,gasout}$/°C	t_{e1}/°C	t_{e2}/°C	t_{e3}/°C	$t_{e1,gasout}$/°C	t_{c1}/°C	t_{c2}/°C	t_g/°C	x_s/%	x_w/%
η_{th}	200	100	120	10	40	140	40	90	35	64	60
COP	200	100	120	20	40	160	30	70	35	52	48
Π	200	100	120	20	40	160	30	90	35	52	48

4. Conclusions

In this paper, a new type of cogeneration system suitable for different scenarios is proposed and focuses on analyzing the impact of different factors on system parameters and performance indexes based on the first law of thermodynamics. At the same time, it is also compared with traditional ORC, compression heat pump, and absorption heat pump to determine the optimal operating conditions of the system in different scenarios. The following conclusions can be obtained:

(1) The factors of flue gas temperature at evaporator1 outlet and CHP have the greatest effect on the parameters and performance indexes of the OACCHP system.
(2) The effect of AHP on the parameters and performance indexes of the OACCHP system can be ignored.
(3) In the given range of flue gas temperature at evaporator1 outlet, the heat production of total and net work is reduced by 1.17% and 33.33%, respectively. In a given range of CHP evaporation temperature, the heat production of the total is reduced by 5.74%.

In the given range of the outlet temperature of the gas cooler, the heat production of the total is increased by 10.58%.

(4) In a given working condition, compared with the single ORC system, the single CHP system, and the single AHP system, the thermal efficiency, COP, and energy earning rate of the OACCHP system are increased by up to 755.49%, 59.8%, and 5.8%, respectively.
(5) For the power generation scenarios, the flue gas temperature at the evaporator1 outlet and the condensation temperature of ORC should be appropriately reduced.
(6) For the heating scenarios, the flue gas temperature at the evaporator1 outlet, the LiBr strong solution concentration, the condensation temperature of AHP should be appropriately reduced, and the condensation temperature of ORC, the bleeding range, the evaporation temperature of AHP, the evaporation temperature of CHP, and the outlet temperature of gas cooler should be appropriately increased.
(7) When increasing COP of the OACCHP system is the main purpose, the flue gas temperature at evaporator1 outlet and the evaporation temperature of CHP should be increased, and the outlet temperature of the gas cooler should be reduced.
(8) When increasing the thermal efficiency of the OACCHP system is the main purpose, the evaporation temperature of CHP should be decreased.
(9) When increasing the energy earning rate of the OACCHP system is the main purpose, the condensation temperature of AHP should be increased, and the evaporation temperature of AHP should be reduced.

In conclusion, the new cogeneration system can meet different application scenarios and purposes, and it is more energy efficient than the system of ORC, CHP, and AHP. It provides a certain reference for the utilization of waste heat resources and the development of cogeneration systems in the future, and also makes a certain contribution to energy saving and emission reduction. In the future, the reliability of the model will be further verified by establishing an experimental platform, and the economy and exergy of the new system will be analyzed.

Author Contributions: Methodology, Z.L.; Investigation, H.Z.; Data curation, X.Z.; Writing—original draft, D.S. All authors have read and agreed to the published version of the manuscript.

Funding: This research received no external funding.

Data Availability Statement: Data is unavailable due to privacy.

Conflicts of Interest: We declare that we have no financial and personal relationships with other people or organizations that can inappropriately influence our work, there is no professional or other personal interest of any nature or kind in any product, service and/or company that could be construed as influencing the position presented in, or the review of, the manuscript entitled.

Nomenclature

E	energy
f	circulation ratio
h	specific enthalpy of state point, kJ/kg
m	mass flow, kg/s
P	pressure, MPa
Q	refrigerating capacity, kW
s	specific entropy of state point, kJ/(kg·K)
t	temperature, °C
W	work input to compressor, kW
x	concentration, %

Greek symbols	
ε	efficiency of compressor
η	efficiency
ΔX	bleeding range
Π	energy earnings coefficient
Subscripts	
number	state point
a	absorber
*c*1	condenser of ORC
*c*2	condenser of AHP
com	compressor
dis	discharge
*e*1	evaporation of ORC
*e*2	evaporation of CHP
*e*3	evaporation of AHP
ex	heat echanger of AHP
g	gas cooler
gas	waste heat flue gas
gex	gas heat exchanger
gain	output of system
ge	generator
gen	power generation
h	heating
in	inlet
n	net
out	outlet
opt	optimal
pump	working fluid pump of orc
pay	input of system
s	strong solution
sys	ORC-AHP-CHP system
t	turbine or expander
th	thermal
wa	water
w	weak solution
Acronyms	
AHP	absorption heat pump
COP	coefficient of performance
CHP	compression heat pump
GWP	global warming potential
ODP	ozone depleting potential
ORC	organic Rankine cycle
OACCHP	ORC-AHP-CHP coupled system

References

1. Lakew, A.A.; Bolland, O. Working fluids for low-temperature heat source. *Appl. Therm. Eng.* **2010**, *30*, 1262–1268. [CrossRef]
2. Zhang, S.J.; Wang, H.X.; Tao, G. Performance comparison and parametric optimization of subcritical Organic Rankine Cycle (ORC) and transcritical power cycle system for low-temperature geothermal power generation. *Appl. Energy* **2011**, *88*, 2740–2754.
3. Wang, H.L.; Peterson, R.; Herron, T. Design study of configurations on system COP for a combined ORC (organic Rankine cycle) and VCC (vapor compression cycle). *Energy* **2011**, *36*, 4809–4820.
4. Sprouse, I.C.; Depcik, C. Review of organic Rankine cycles for internal combustion engine exhaust waste heat recovery. *Appl. Therm. Eng.* **2013**, *51*, 711–722. [CrossRef]
5. Maraver, D.; Sin, A.; Royo, J.; Sebastián, F. Assessment of CCHP systems based on biomass combustion for small-scale applications through a review of the technology and analysis of energy efficiency parameters. *Appl. Energy* **2013**, *102*, 1303–1313. [CrossRef]
6. Mohammadi, A.; Ahmadi, M.H.; Bidi, M.; Joda, F.; Valero, A.; Uson, S. Exergy analysis of a combined cooling, heating and power system integrated with wind turbine and compressed air energy storage system. *Energy Convers. Manag.* **2017**, *131*, 69–78. [CrossRef]

7. Brueckner, S.; Miro, L.; Cabeza, L.F.; Pehnt, M.; Laevemann, E. Methods to estimate the industrial waste heat potential of regions-A categorization and literature review. Renew. *Sustain. Energy Rev.* **2014**, *38*, 164–171. [CrossRef]
8. Song, J.; Song, Y.; Gu, C.W. Thermodynamic analysis and performance optimization of an Organic Rankine Cycle (ORC) waste heat recovery system for marine diesel engines. *Energy Convers. Manag.* **2015**, *82*, 976–985. [CrossRef]
9. Mikielewicz, D.; Wajs, J.; Ziółkowski, P.; Mikielewicz, J. Utilisation of waste heat from the power plant by use of the ORC aided with bleed steam and extra source of heat. *Energy* **2016**, *97*, 11–19. [CrossRef]
10. Loni, R.; Najafi, G.; Bellos, E.; Rajaee, F.; Said, Z.; Mazlan, M. A review of industrial waste heat recovery system for power generation with Organic Rankine Cycle: Recent challenges and future outlook. *J. Clean. Prod.* **2021**, *287*, 125070.
11. Sun, D.H.; Liu, Z.Y.; Zhang, H.; Zhang, X. Performance analysis of a new mechanical superheat coupled-orc refrigeration system with thermoelectric conversion. *Appl. Therm. Eng.* **2023**, *229*, 120627. [CrossRef]
12. Nondy, J.; Gogoi, T.K. Exergoeconomic investigation and multi-objective optimization of different ORC configurations for waste heat recovery: A comparative study. *Energy Convers. Manag.* **2021**, *245*, 114593. [CrossRef]
13. Soltani, M.; Nabat, M.H.; Razmi, A.R.; Dusseault, M.B.; Nathwani, J. A comparative study between ORC and Kalina based waste heat recovery cycles applied to a green compressed air energy storage (CAES) system. *Energy Convers. Manag.* **2020**, *222*, 113203. [CrossRef]
14. Wang, F.; Wang, L.; Zhang, H.C.; Xia, L.; Miao, H.; Yuan, J.L. Design and optimization of hydrogen production by solid oxide electrolyzer with marine engine waste heat recovery and ORC cycle. *Energy Convers. Manag.* **2021**, *229*, 113775. [CrossRef]
15. Wei, D.H.; Lu, X.S.; Lu, Z.; Gu, J.M. Performance analysis and optimization of organic Rankine cycle (ORC) for waste heat recovery. *Energy Convers. Manag.* **2007**, *48*, 1113–1119. [CrossRef]
16. Wang, E.H.; Zhang, H.G.; Fan, B.Y.; Ouyang, M.G.; Zhao, Y.; Mu, Q.H. Study of working fluid selection of organic Rankine cycle (ORC) for engine waste heat recovery. *Energy* **2011**, *36*, 3406–3418. [CrossRef]
17. Alghamdi, M.; AI-Kharsan, I.; Shahab, S.; Albaker, A.; Alayi, R.; Kumar, L.; Assad ME, H. Investigation of Energy and Exergy of Geothermal Organic Rankine Cycle. *Energies* **2023**, *16*, 2222. [CrossRef]
18. Cao, X.Q.; Yang, W.W.; Zhou, F.; He, Y.L. Performance analysis of different high-temperature heat pump systems for low-grade waste heat recovery. *Appl. Therm. Eng.* **2014**, *71*, 291–300. [CrossRef]
19. Hu, B.; Liu, H.; Jiang, J.T.; Zhang, Z.P.; Li, H.B.; Wang, R.Z. Ten megawatt scale vapor compression heat pump for low temperature waste heat recovery: Onsite application research. *Energy* **2022**, *238*, 121699. [CrossRef]
20. Mateu-Royo, C.; Arpagaus, C.; Mota-babiloni, A.; Navarro-Esbri, J.; Bertsch, S.S. Advanced high temperature heat pump configurations using low GWP refrigerants for industrial waste heat recovery: A comprehensive study. *Energy Convers. Manag.* **2021**, *229*, 113752. [CrossRef]
21. Hou, J.; Che, D.; Liu, Y.; Jiang, Q.W. A new system of absorption heat pump vs boiler for recovering heat and water vapor in flue gas. *Energy Procedia* **2018**, *152*, 1266–1271. [CrossRef]
22. Lars, W.; Roger, H.; Jonathan, F. Flue gas purification and heat recovery: A biomass fired boiler supplied with an open absorption system. *Appl. Energy* **2012**, *96*, 444–450.
23. Xu, Z.Y.; Gao, J.T.; Mao, H.C. Double-section absorption heat pump for the deep recovery of low-grade waste heat. *Energy Convers. Manag.* **2020**, *220*, 113072. [CrossRef]
24. Ma, Z.; Bao, H.; Roskilly, A.P. Numerical studyof ahybrid absorption-compression high temperature heat pump for industrial waste heat recovery. *Front. Energy* **2017**, *11*, 503–509. [CrossRef]
25. Yang, S.; Deng, C.; Liu, Z. Optimal design and analysis of a cascade LiBr/H_2O absorption refrigeration/transcritical CO_2 process for low-grade waste heat recovery. *Energy Convers. Manag.* **2019**, *192*, 232–242. [CrossRef]
26. Sun, J.; Ge, Z.H.; Fu, L. Investigation on LiBr-H_2O double evaporation-absorption heat pump (DEAHP) for heat recovery under lower driving sources. *Appl. Therm. Eng.* **2017**, *125*, 978–985. [CrossRef]
27. Assad, M.E.H.; Sadeghzadeh, M.; Ahmadi, M.H.; Al-Shabi, M.; Albawab, M.; Anvari-Moghaddam, A.; Hani, E.B. Space cooling using geothermal single-effect water/lithium bromide absorption chiller. *Energy Sci. Eng.* **2021**, *9*, 1747–1760. [CrossRef]
28. Chang, H.W.; Wan, Z.M.; Zheng, Y.; Chen, X.; Shu, S.M.; Tu, Z.K.; Chan, S.H. Energy-and exergy-based working fluid selection and performance analysis of a high-temperature PEMFC-based micro combined cooling heating and power system. *Appl. Energy* **2017**, *204*, 446–458. [CrossRef]
29. Pan, M.A.; Lu, F.L.; Zhu, Y.; Huang, G.C.; Yin, J.W.; Huang, F.C.; Chen, G.S. Thermodynamic, exergoeconomic and multi-objective optimization analysis of new ORC and heat pump system for waste heat recovery in waste-to-energy combined heat and power plant. *Energy Convers. Manag.* **2020**, *222*, 113200. [CrossRef]
30. Ebrahimi-Moghadam, A.; Moghadam, A.J.; Farzaneh-Gord, M. Comprehensive techno-economic and environmental sensitivity analysis and multi-objective optimization of a novel heat and power system for natural gas city gate stations. *J. Clean. Prod.* **2020**, *262*, 121261.
31. Xie, D.; Wang, Z.; Jin, L.; Zhang, Y. Energy and exergy analysis of a fuel cell based micro combined heat and power cogeneration system. *Energy Build.* **2012**, *50*, 266–272. [CrossRef]
32. Obi, J.B. State of Art on ORC Applications for Waste Heat Recovery and Micro-cogeneration for Installations up to 100kW. *Energy Procedia* **2015**, *82*, 994–1001. [CrossRef]
33. Holik, M.; Zivic, M.; Virag, Z.; Barac, A.; Vujanovic, M.; Avsec, J. Thermo-economic optimization of a Rankine cycle used for waste-heat recovery in biogas cogeneration plants. *Energy Convers. Manag.* **2021**, *232*, 113897. [CrossRef]

34. Pantaleo, A.M.; Fordham, J.; Oyewunmi, O.A.; Palma, P.D.; Markides, C.N. Integrating cogeneration and intermittent waste-heat recovery in food processing: Microturbines vs. ORC systems in the coffee roasting industry. *Appl. Energy* **2018**, *225*, 782–796. [CrossRef]
35. Su, Z.X.; Yang, L. A novel and efficient cogeneration system of waste heat recovery integrated carbon capture and dehumidification for coal-fired power plants. *Energy Convers. Manag.* **2022**, *255*, 115358. [CrossRef]
36. Liu, L.C.; Wu, J.L.; Zhong, F.; Gao, N.P.; Cui, G.M. Development of a novel cogeneration system by combing organic rankine cycle and heat pump cycle for waste heat recovery. *Energy* **2021**, *217*, 119445. [CrossRef]
37. Zhang, H.S.; Zhao, H.B.; Li, Z.L. Waste heat recovery and water-saving modification for a water-cooled gas-steam combined cycle cogeneration system with absorption heat pump. *Energy Convers. Manag.* **2019**, *180*, 1129–1138. [CrossRef]
38. Li, Y.; An, H.L.; Li, W.T.; Zhang, S.Y.; Jia, X.Q.; Fu, L. Thermodynamic, energy consumption and economic analyses of the novel cogeneration heating system based on condensed waste heat recovery. *Energy Convers. Manag.* **2018**, *117*, 671–681. [CrossRef]
39. Lemmon, E.; McLinden, M.; Huber, M. *NIST Standard Reference Database 23. Reference Fluid Thermodynamic and Transport Properties Database (REFPROP)*, 9th ed.; National Institute of Standards and Technology (NIST): Gaithersburg, MD, USA, 2010.
40. Sarkar, J.; Bhattacharyya, S.; Gopal, M.R. Optimization of a transcritical CO_2 heat pump cycle for simultaneous cooler and heating applications. *Int. J. Refrig.* **2004**, *27*, 830–838. [CrossRef]
41. Vaja, I.; Gambarotta, A. Internal Combustion Engine (ICE) bottoming with Organic Rankine Cycles (ORCs). *Energy* **2010**, *35*, 1084–1093. [CrossRef]
42. Salim, M.S.; Kim, M.H. Multi-objective thermo-economic optimization of a combined organic Rankine cycle and vapour compression refrigeration cycle. *Energy Convers. Manag.* **2019**, *199*, 112054. [CrossRef]
43. Wang, Y. Performance Study of Biomass Flue Gas Waste Heat Recovery System Based on Absorption-Compression Compound Heat Pumps. Master's Thesis, Northeast Electric Power University, Jilin, China, 2022.

Disclaimer/Publisher's Note: The statements, opinions and data contained in all publications are solely those of the individual author(s) and contributor(s) and not of MDPI and/or the editor(s). MDPI and/or the editor(s) disclaim responsibility for any injury to people or property resulting from any ideas, methods, instructions or products referred to in the content.